J. Fluid Mech. (2015), *vol.* 766, *pp.* 528–555. © Cambridge University Press 2015
doi:10.1017/jfm.2014.711

Transition to stably stratified states in open channel flow with radiative surface heating

N. Williamson[1,†], S. W. Armfield[1], M. P. Kirkpatrick[1] and S. E. Norris[2]

[1]School of Aerospace, Mechanical and Mechatronic Engineering, University of Sydney, NSW 2006, Australia

[2]Department of Mechanical Engineering, University of Auckland, Auckland, New Zealand

(Received 16 December 2013; revised 29 August 2014; accepted 4 December 2014; first published online 9 February 2015)

Direct numerical simulations (DNS) of turbulent stratified flow in an open channel with an internal heat source following the Beer–Lambert law from the surface are used to investigate the transition from neutral to strongly stable flow. Our buoyancy bulk parameter is defined through the ratio of the domain height δ to $\mathscr{L}$, a bulk Obukhov length scale for the flow. We cover the range $\lambda = \delta/\mathscr{L} = 0$–$2.0$, from neutral conditions to the onset of the stable regime, with the Reynolds number range $Re_\tau = 200$–800, at a Prandtl number of 0.71. The result is a boundary layer flow where the effects of stratification are weak in the wall region but progressively stronger in the outer layer up to the free surface. At $\lambda \simeq 1$ the turbulent kinetic energy (TKE) budget is in local equilibrium over a region extending from the near-wall region to a free-surface affected region a distance l_ν from the surface, with $l_\nu/\delta \sim Re^{-1/2}$. In this equilibrium region the flow can be characterised by the flux Richardson number R_f and the local Obukhov length scale Λ. At higher λ local mixing limit conditions are observed over an extended region. At $\lambda = 2$ the flux Richardson number approaches critical limit values of $R_{f,c} \simeq 0.18$ and gradient Richardson number $Ri_c \simeq 0.2$. At high λ, we obtain a flow field where buoyancy interacts with the smallest scales of motion and the turbulent shear stress and buoyancy flux are suppressed to molecular levels. We find that this regime can be identified in terms of the parameter $Re_{\mathscr{L},c} = \mathscr{L}u_\tau/\nu \lesssim 200$–$400$ (where u_τ is the friction velocity and ν the kinematic viscosity), which is related to the L_* parameter of Flores and Riley (*Boundary-Layer Meteorol.*, vol. 139 (2), 2011, pp. 241–259) and buoyancy Reynolds number $\mathscr{R}$. With energetic equilibrium attained, the local buoyancy Reynolds number, $Re_\Lambda = \Lambda\langle u'w'\rangle^{1/2}/\nu$, is directly related to the separation of the Ozmidov (l_O) and Kolmogorov (η) length scales in the outer boundary layer by $Re_\Lambda \simeq \mathscr{R} \equiv (l_O/\eta)^{4/3}$. The inner wall region has the behaviour $\mathscr{R} \sim Re_\mathscr{L} Re_\tau$, in contrast to stratified boundary layer flows where the buoyancy flux is non-zero at the wall and $\mathscr{R} \sim Re_\mathscr{L}$.

Key words: geophysical and geological flows, mixing and dispersion, stratified turbulence

1. Introduction

We examine turbulent stably stratified open channel flow as a canonical representation of flow in rivers and to some extent flow in estuaries and continental

† Email address for correspondence: nicholas.williamson@sydney.edu.au

shelf seas. Where incident solar radiation penetrates the water column, the transmission and absorption of the radiation, following the Beer–Lambert law, can produce a stable thermocline near the free surface, whereas the near-wall region remains relatively unaffected by stratification. Relating the dynamics of the interior structure in these flows to known outer bulk parameters is very important. For example, in periods of drought or below average flow, Australian inland rivers can become thermally stratified to the extent that algal blooms may occur and oxygen or nutrient transport can be reduced, adversely affecting river biota and water quality. With reliable forecasting models these events may be predicted and mitigated against.

Simpson & Hunter (1974) proposed that in continental shelf seas, a constant fraction of the work done by tidal stresses acting on the seabed is available to mix the stratified surface layer and that this mechanical work can be compared with surface heat input to form a critical parameter for the onset of stratification. Similar interpretations have been proposed as a metric to delineate stratified and non-stratified flow regimes in estuaries (Holloway 1980), river flows (Bormans & Webster 1997) and in wind-induced surface mixing in the ocean (Kullenberg 1976; Simpson, Allen & Morris 1978). The total work input to the domain ($\dot{W}$) and the rate at which potential energy ($\dot{E}p$) must be increased to maintain a mixed column in steady conditions can be written

$$\dot{W} = \tau_w u_b = u_b^3 C_f \frac{1}{2}\rho_0 = \rho_0 u_\tau^3 \sqrt{\frac{2}{C_f}}, \quad \dot{E}p = \frac{g\beta}{C_p}\delta^2 q_N, \tag{1.1a,b}$$

where C_f is the skin friction coefficient, u_b is the bulk or volume-average velocity, ρ_0 is the fluid density, τ_w is the wall shear stress, u_τ is the friction velocity, g is the gravitational acceleration, C_p is the specific heat, δ is the domain height, β is the coefficient of thermal expansion, $q(z)$ is the depth-varying volumetric heat source in the water column and

$$q_N = \frac{1}{\delta^2}\int_0^\delta (\overline{q} - q(z))(z-\delta)\mathrm{d}z, \quad \overline{q} = \frac{1}{\delta}\int_0^\delta q(z)\mathrm{d}z. \tag{1.2a,b}$$

Combining (1.1*a*,*b*) gives the ratio

$$E_r = \frac{\dot{E}p}{\dot{W}} = \frac{g\beta}{\rho_0 C_p u_\tau^3}\delta^2 q_N \sqrt{\frac{C_f}{2}}. \tag{1.3}$$

In the setting shown in figure 1, I_s is the radiant heat flux through the surface, α is the absorption coefficient following the Beer–Lambert law, so

$$q(z) = I_s \alpha \mathrm{e}^{(\delta - z)\alpha}, \tag{1.4}$$

and for large $\alpha\delta$, E_r can be reduced to

$$E_r \simeq \frac{g\beta}{\rho_0 C_p u_\tau^3}\delta I_s \left(\frac{1}{2} - \frac{1}{\delta\alpha}\right)\sqrt{\frac{C_f}{2}}. \tag{1.5}$$

In coastal seas the critical values for the onset of stratification, determined by the location of seasonal thermal fronts, are typically $E_{rc} \simeq 0.003$ (Garrett, Keeley & Greenberg 1978; Hearn 1985) for tidal mixing. Simpson & Hunter (1974) originally

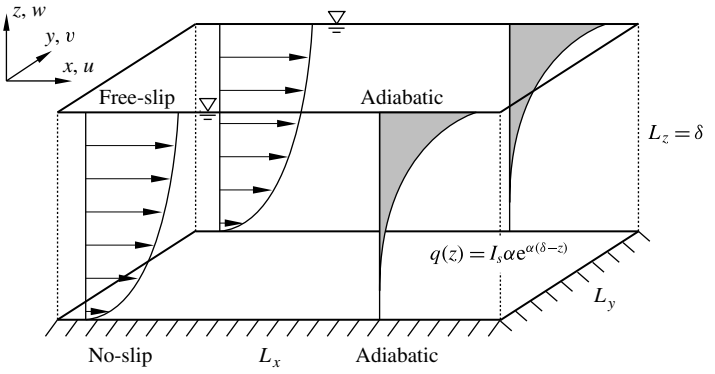

FIGURE 1. Schematic of the flow; the domain is periodic in x and y.

found $E_{rc} = 0.0037$ and Bormans & Webster (1997) reported $E_{rc} = 0.0044$ in mixing in a river weir pool. It is not clear how the internal structure of the flow varies with the outer parameter E_r or how general E_{rc} is across other parameters, Reynolds and Prandtl numbers Re, Pr, or $\alpha\beta$. These effects may be important at the reduced scale of some small river canals. It is clear that E_{rc} is several orders of magnitude smaller than limit values of local flux Richardson number R_f, a measure of local mixing efficiency.

The influence of stratification in the atmospheric surface layer is characterised by the ratio of the Obukhov length scale $L = u_\tau^3/\kappa b_*$, where κ is the von-Kaŕmań constant and b_* is the surface buoyancy flux, to a confinement scale which in the surface layer is z (e.g. Monin 1970; Chung & Matheou 2012). This ratio $\zeta = z/L$ indicates that the flow is affected by stratification for $\zeta \gtrsim 1$, while for $\zeta \ll 1$ the flow approaches neutral conditions. For the current configuration, a bulk stability parameter λ (cf. E_r) can also be defined in terms of bulk Obukhov length scale $\mathscr{L}$ and confinement scale δ consistent with this approach and (1.5):

$$\lambda = \delta/\mathscr{L}, \quad \mathscr{L} = \frac{u_\tau^3}{g\beta I_s/\rho_0 C_p}\left(\frac{1}{2} - \frac{1}{\delta\alpha}\right)^{-1}. \tag{1.6a,b}$$

Outside the surface layer the localised Obukhov length scale, $\Lambda(z)$ (Nieuwstadt 1984; Sorbjan 1986; Chung & Matheou 2012) can be defined in terms of fluxes as

$$\zeta(z) = \xi/\Lambda(z), \quad \Lambda(z) = \langle u'w' \rangle^{3/2}/\langle b'w' \rangle, \tag{1.7a,b}$$

where ξ is a local confinement scale such as z, the buoyancy fluctuation is $b' = g\rho'/\rho_0$, $\langle\,\rangle$ denotes temporal averaging and the prime denotes a perturbation from the mean. Recent efforts to parameterise the effects of stratification on mixing in turbulent flow (Ivey & Imberger 1991; Holt, Koseff & Ferziger 1992; Itsweire *et al.* 1993; Barry *et al.* 2001; Shih *et al.* 2005; Lindborg 2006; Brethouwer *et al.* 2007; Gonzalez-Juez, Kerstein & Shih 2011; Chung & Matheou 2012) have demonstrated that multiple regimes of behaviour exist, which can be related to two non-dimensional parameters: the buoyancy Reynolds number $\mathscr{R}$ (Dillon & Caldwell 1980; Gargett, Osborn & Nasmyth 1984; Itsweire *et al.* 1993) and the gradient Richardson number Ri,

$$\mathscr{R} = \frac{\epsilon}{\nu N^2} = \left(\frac{l_O}{\eta}\right)^{4/3}, \quad Ri = \frac{N^2}{S^2} = \left(\frac{l_C}{l_O}\right)^{4/3}. \tag{1.8a,b}$$

These parameters can be formed out of characteristic length scales in stratified turbulent flow (Smyth & Moum 2000; Brethouwer *et al.* 2007; Chung & Matheou 2012): the Ozmidov length scale l_O, the length scale above which the effects of buoyancy are strongly felt; the Kolmogorov length scale η, which characterises the smallest scales of motion; and the Corrsin scale l_C, the length scale characterising the smallest eddies which interact with background shear,

$$l_C = \left(\frac{\epsilon}{S^3}\right)^{1/2}, \quad l_O = \left(\frac{\epsilon}{N^3}\right)^{1/2}, \quad \eta = \left(\frac{\nu^3}{\epsilon}\right)^{1/4}, \tag{1.9a–c}$$

where $N^2 = (-g/\rho)(\mathrm{d}\langle\rho\rangle/\mathrm{d}z)$, $S = (\mathrm{d}\langle U\rangle/\mathrm{d}z)$, the turbulent dissipation rate $\epsilon = \nu\langle(\partial u_i'/\partial x_j)^2\rangle$ and ν is the kinematic viscosity.

In the limit $Ri \to 0$, $l_O \gg l_C$, the flow approaches neutral conditions and the flow is characterised by l_C and η (Smyth & Moum 2000). With increasing stability (decreasing l_O), for $l_O > l_C > \eta$, the flow approaches a regime of constant, maximum mixing efficiency and Ri approaches a critical value $Ri_c \simeq 0.2$–0.25 (Holt *et al.* 1992; Chung & Matheou 2012). Scales between l_O and η are weakly affected by stratification while those larger than l_O are strongly affected, leading to modification of the classical energy cascade in turbulent flow (Lindborg 2006; Brethouwer *et al.* 2007). Further, with increasing stability the flow approaches a regime where buoyancy affects the smallest scales of motions (Brethouwer *et al.* 2007) and turbulent mixing is strongly suppressed by buoyancy (Itsweire *et al.* 1993; Barry *et al.* 2001; Shih *et al.* 2005; Brethouwer *et al.* 2007; Ivey, Winters & Koseff 2008; Gonzalez-Juez *et al.* 2011). Brethouwer *et al.* (2007) found $\mathscr{R}_c \simeq 1$ a sufficient criterion for the onset of this behaviour. In the atmospheric surface layer, the collapse of turbulence was found by Flores & Riley (2011) to be characterised by a related parameter $L_* = Lu_\tau/\nu$ in the terms of the Obukhov length scale, and found a critical limit of $L_{*,c} \lesssim 100$.

The description of the state of stratified turbulence then requires an outer buoyancy parameter, such as Ri or λ, and a parameter related to ν, such as $\mathscr{R}$ or L_* (Chung & Matheou 2012). For the present flow the equivalent definitions of L_* for bulk and local parameters can be defined as

$$Re_{\mathscr{L}} = \mathscr{L}u_\tau/\nu, \quad Re_\Lambda(z) = \Lambda\langle u'w'\rangle^{1/2}/\nu. \tag{1.10a,b}$$

We then define our problem, as outlined in figure 1, in terms of the parameter set $(\alpha\delta, \lambda, Re_\tau, Pr)$ with the friction Reynolds number $Re_\tau = u_\tau\delta/\nu$, or equivalently the set $(\alpha\delta, \lambda, Re_{\mathscr{L}}, Pr)$ with $Re_{\mathscr{L}} \equiv Re_\tau/\lambda$. We have acknowledged a Prandtl number dependence (Barry *et al.* 2001; Shih *et al.* 2005; Gonzalez-Juez *et al.* 2011) here but confine our study to fixed $Pr = 0.71$. The objective of the study is to examine how local flow character varies with these bulk parameters and in terms of the local parameters defined in (1.8).

We describe our method in § 2 and in § 3 we show that we are able to attain a statistically steady flow field over a wide range of stability ratios and, unlike most previous studies, the near-wall region remains only very weakly affected by buoyancy. In § 4.1 we show that $\lambda \simeq 1$ indicates a transition to strongly stratified flow and for $\lambda \gtrsim 1$ the flow is in local energetic equilibrium. In § 4.2 we show that $Re_{\mathscr{L}} \simeq 200$–$400$ is associated with the onset of the weakly turbulent $\mathscr{R} < \mathscr{R}_c$ regime in the outer boundary layer and that the onset of local equilibrium conditions allows a direct relationship between $\mathscr{R}$ and $Re_\Lambda(z)$ to be obtained. In § 4.3 we conclude that the parameter set $(\lambda, Re_{\mathscr{L}})$ is more relevant for describing the dynamics of the flow than E_r. In § 4.4

we identify these transition behaviours in terms of the turbulent eddy viscosity k_m. The outer extremities of the channel – the near-wall region and the free surface – impose other length scale restrictions on the flow. In § 5 we examine the scaling for $\mathscr{R}$ in the near-wall region and show that $\mathscr{R} \sim Re_{\mathscr{L}} Re_\tau$, rather than the $\mathscr{R} \sim Re_{\mathscr{L}}$ which holds in stratified boundary layer flows where the buoyancy flux is non-zero at the wall, leading to a wider separation of viscous- and buoyancy-affected scales at the wall in the present configuration. In § 6 we consider the modifications to the scaling for the length of the near-free-surface affected region under stratified conditions.

2. Problem formulation

We approach this problem by obtaining a numerical simulation of the flow illustrated in figure 1. The flow is periodic in the horizontal plane and driven by a constant pressure gradient. A volumetric heat source, following (1.4), is applied to the flow. In our canonical model we assume no heat is lost through the lower wall or the stress-free surface, which are taken as adiabatic. After an initial transient period the flow attains a statistically steady horizontally homogeneous state and the energy input from the source term is transported across the channel at a constant rate, so the dimensional temperature field Φ at time T can be decomposed into

$$\Phi(x, T) = \Phi'(x, T) + \overline{\Phi}(T), \tag{2.1}$$

where Φ' is the statistically steady temperature field and the uniform increase in temperature with time is

$$\partial\overline{\Phi}/\partial T = \overline{q}/\rho_0 C_p. \tag{2.2}$$

With this reference frame we obtain a non-dimensional statistically steady temperature field (ϕ) and depth-varying heat source (qe) by normalising $\Phi_N = q_N \delta/\rho_0 C_p u_\tau$ and q_N (defined in (1.2)) respectively,

$$\phi = \frac{(\Phi - \overline{\Phi}(T))}{\Phi_N}, \quad qe(z) = \frac{(q(z) - \overline{q})}{q_N}. \tag{2.3a,b}$$

With this normalisation we perform direct numerical simulations (DNS) of the Navier–Stokes equations. We consider an incompressible fluid with the Oberbeck–Boussinesq approximation for buoyancy. The governing equations for the conservation of mass, momentum and energy are written in non-dimensional form as

$$\nabla \cdot \boldsymbol{u} = 0, \tag{2.4}$$

$$\frac{\partial \boldsymbol{u}}{\partial t} + \nabla \cdot (\boldsymbol{u}\boldsymbol{u}) = -\nabla p + \frac{1}{Re_\tau}\nabla^2 \boldsymbol{u} + \boldsymbol{e}_x + \lambda\phi \boldsymbol{e}_z, \tag{2.5}$$

and

$$\frac{\partial \phi}{\partial t} + \nabla \cdot (\boldsymbol{u}\phi) = \frac{1}{Re_\tau Pr}\nabla^2 \phi + qe, \tag{2.6}$$

where $\boldsymbol{e}_x$ and $\boldsymbol{e}_z$ are the unit vectors in the x and z directions. The Prandtl number $Pr = \nu/\sigma = 0.71$, where σ is the scalar diffusivity of the fluid. With this non-dimensional form, the velocity field is normalised by u_τ which is set through the specified $Re_\tau = u_\tau \delta/\nu$ and the constant imposed pressure gradient in the streamwise direction, $\boldsymbol{e}_x$. The length, time and pressure are made non-dimensional by δ, u_τ and ρ_0, a reference density. In specifying the problem, Re_τ and λ are given and, together

with $\alpha\delta$ (specified in (1.4)) and Pr, fully describe the problem. In this scheme the surface flux I_s which occurs in (1.4) is a free variable which scales the temperature field. In presenting the results, we re-normalise the temperature field by either I_s or the bulk temperature difference $\Delta\phi = \phi_1 - \phi_0$, where ϕ_1 and ϕ_0 are the free-surface and wall temperatures respectively. This gives more meaningful normalisation of $\phi_d = \phi/\Delta\phi$ or $\phi_i = \phi/(I_s/\delta q_N)$.

The boundary conditions for the bottom ($z = 0$) no-slip adiabatic wall and stress-free adiabatic top boundary ($z = 1$) are

$$z = 0: \quad u = v = w = 0, \quad \frac{\partial \phi}{\partial z} = 0, \tag{2.7}$$

$$z = 1: \quad \frac{\partial u}{\partial z} = \frac{\partial v}{\partial z} = w = 0, \quad \frac{\partial \phi}{\partial z} = 0. \tag{2.8}$$

2.1. *DNS*

The equations are solved using the fractional-step finite-volume solver described in Armfield *et al.* (2002). The code uses a cell-centred co-located storage arrangement for flow variables on a regular structured grid, with cell-face velocities calculated using the Rhie–Chow momentum interpolation. The spatial derivatives are discretised using second-order central finite differences. A second-order-accurate Adams–Bashforth time advancement scheme is used for the nonlinear terms and Crank–Nicolson for the time advancement of the diffusive terms. The pressure correction equation is solved using a stabilised bi-conjugate gradient solver with an incomplete Cholesky factorisation pre-conditioner. The momentum and temperature equations are solved using a Jacobi solver. A Courant number limit of 0.2–0.24 is used to obtain the time step size.

The simulation parameters are given in table 1. We perform simulations from neutral ($\lambda = 0$) to stable conditions ($\lambda = 0.05$–2.0) at $Re_\tau = 395$ and $\alpha\delta = 8$. We demonstrate a sufficient range to determine the transition to a high-λ flow structure where critical values of Ri are achieved in the channel core and the turbulent kinetic energy (TKE) balance is in local equilibrium. Additional simulations are performed at higher and lower Reynolds number $Re_\tau = 200$–800 and at $\alpha\delta = 32$. Unless otherwise stated, results are for $Re_\tau = 395$, $\alpha\delta = 8$.

The Kolmogorov length scale, expressed in viscous wall units $\eta^+ = Re_\tau \eta/\delta$, ranges over $\eta^+ = 1.5$–4.7 (shown in § 5). At $Re_\tau = 395$, the grid size is set at $\Delta x^+ = 10$ ($N_x = 256$), $\Delta y^+ = 5$ ($N_y = 256$) for $\lambda = 0$–0.5. In the vertical axis, the grid is stretched from $\Delta z^+ = 0.4$ at the wall to $\Delta z^+ = 3.95$ at $z = 0.6$ and from $z = 0.6$–1 the grid is uniform with $\Delta z^+ = 3.95$ ($N_z = 110$). At $\lambda = 1.0$–2.0 the grid was refined to $\Delta x^+ = 4.68$ ($N_x = 540$) and in the vertical $\Delta z^+ = 0.4$–4.1 with the grid stretched to $\Delta z^+ = 1.1$ at the free surface ($N_z = 130$). At $\alpha\delta = 32$, this vertical resolution is also used. The single simulation at $Re_\tau = 800$ has $\Delta x^+ = 10$, $\Delta y^+ = 5$ and $\Delta z^+ = 0.4$–4.0. The accuracy of the results has been verified in neutral conditions against benchmark DNS solutions of Abe, Kawamura & Matsuo (2001) and Moser, Kim & Mansour (1999) for closed channel flow at $Re = 395$.

Initial simulations were performed at neutral conditions. After an initial transient phase, typically $\Delta t = 30$–40 (non-dimensional time units δ/Tu_τ), statistically steady conditions were judged to have been obtained. This was determined by convergence of zeroth- and second-order moments of temperature and velocity fluctuations to the mean values and balance of the transport budget for ϕ (see (3.1) below) over the

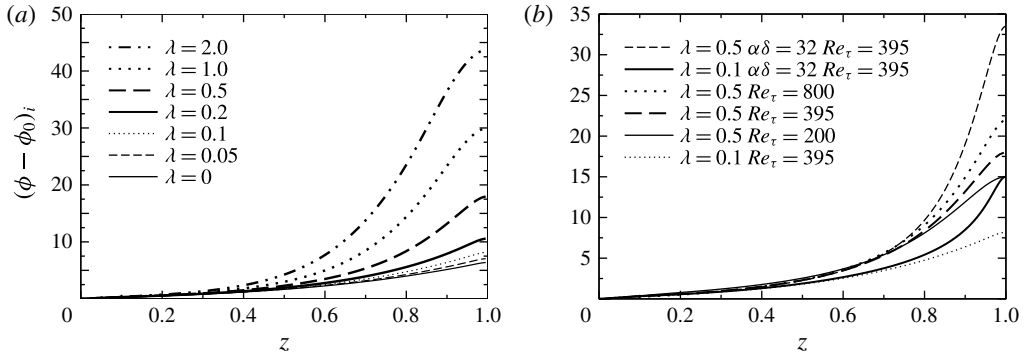

FIGURE 2. Mean temperature profile, $(\phi - \phi_0)/(I_s/\delta q_N)$ at $Re_\tau = 395$, $\alpha\delta = 8$ (a) and $Re_\tau = 200$–800, $\alpha\delta = 8$–32 (b).

λ	Re_τ	$\alpha\delta$	$Re_{\mathscr{L}}$	L_x, L_y	$N_x \times N_y \times N_z$	:	$E_r \times 10^3$	$C_f \times 10^3$	Ri_b	Ri_τ	Re_τ^*
0.0	395	8	0	$2\pi, \pi$	$256 \times 256 \times 110$	:	0.0	6.32	0.0	0	394.68
0.05	395	8	7900	$2\pi, \pi$	$256 \times 256 \times 110$	:	2.79	6.25	0.0029	0.93	395.20
0.1	395	8	3950	$2\pi, \pi$	$256 \times 256 \times 110$	:	5.52	6.10	0.0066	2.16	394.72
0.2	395	8	1975	$2\pi, \pi$	$256 \times 256 \times 110$	:	10.8	5.86	0.0165	5.63	394.80
0.5	395	8	790	$2\pi, \pi$	$256 \times 256 \times 110$	:	25.7	5.27	0.0631	23.9	395.08
1.0	395	8	395	$2\pi, \pi$	$540 \times 256 \times 130$	:	46.5	4.32	0.1725	79.9	395.26
2.0	395	8	197.5	$2\pi, \pi$	$540 \times 256 \times 130$	:	79.5	3.17	0.3693	233	395.46
0.5	200	8	400	$4\pi, 2\pi$	$256 \times 256 \times 80$	:	28.1	6.3	0.0627	20.2	200.20
0.5	800	8	1600	$2\pi, \pi$	$512 \times 512 \times 220$	:	23.0	4.22	0.0618	29.3	800.66
1.0	200	8	200	$8\pi, 4\pi$	$512 \times 512 \times 80$	:	50.3	5.07	0.144	56.8	200.80
0.1	395	32	3950	$2\pi, \pi$	$256 \times 256 \times 130$	:	5.52	6.10	0.0098	3.21	395.24
0.5	395	32	790	$2\pi, \pi$	$256 \times 256 \times 130$	:	25.7	5.28	0.0947	35.9	394.80

TABLE 1. Simulation parameters, and measured flow statistics: $E_r = \lambda\sqrt{C_f/2}$, $C_f = 2(u_\tau/u_b)^2$, $Ri_b = \Delta\phi\lambda\delta/u_b^2$, $Ri_\tau = \Delta\phi\lambda\delta/u_\tau^2$, and Re_τ^* is Reynolds number based on the measured wall friction velocity u_τ^*.

height of the domain. The flow was then evolved for a further period, typically $\Delta t =$ 40–80, with statistics collected. Subsequent higher λ flow conditions were successively initialised from these converged solution flow fields and computations continued in the same manner.

3. Temperature stratification profile

A defining feature of this flow is the separation of the stratified outer layer from the near-wall region so that even at large bulk stability ratio, λ, turbulence production at the wall remains relatively unaffected by buoyancy. In this section we examine this flow structure with reference to the vertical profiles of mean flow statistics, obtained in statistically steady conditions and averaged over a horizontal plane and in time, as denoted by $\langle\cdot\rangle$.

The mean temperature profile normalised by the incident surface flux $(I_s/\delta q_N)$ is shown in figure 2(a) for flow at $Re_\tau = 395$, $\alpha\delta = 8$ and $\lambda = 0$–2.0 while in figure 2(b) the results are compared with flow at $\lambda = 0.5$, $\alpha\delta = 32$, $(Re_\tau = 395)$ and flow at $\lambda = 0.5$, $Re_\tau = 800$. Through the centre of the channel the flow can be separated into a weakly

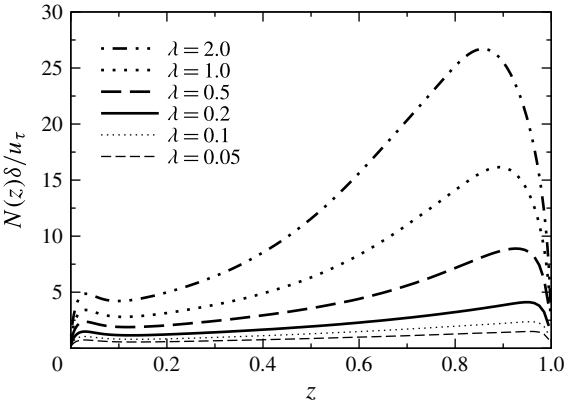

FIGURE 3. Mean buoyancy frequency, $N(z)\delta/u_\tau$ at $Re_\tau = 395$, $\alpha\delta = 8$.

stratified lower mixed region which is insensitive to λ and an outer layer with a thermocline extending almost to the surface. With increasing λ, the thermocline rises more steeply and extends further into the channel. At $\lambda = 1$ it extends from $z \simeq 0.5$ as indicated by the separation from the low-λ profiles. At higher $\alpha\delta = 32$ at both $\lambda = 0.1$ and $\lambda = 0.5$ shown in figure 2(*b*), the near-surface temperature increases significantly for $z \gtrsim 0.75$ as more heat is absorbed in the less turbulent free-surface region. The normalised Brunt–Väisälä frequency ($N\delta/u_\tau$) shown in figure 3 illustrates the same structure. The temperature gradient peaks within the water column over $z \simeq 0.8$–0.97 and goes to zero at the wall and surface as enforced through our adiabatic boundary conditions (2.7) and (2.8).

The variation in the structure of the flow with height and λ can be visualised through realisations of the temperature field as shown in figure 4. Here, in random instances of the flow, ϕ is depicted in the x–z plane for $Re_\tau = 395$ $\lambda = 0.1$–2.0. At $\lambda = 0.1$, in near-neutral conditions, the flow is active throughout the outer boundary layer up to the free surface, with large overturns in ϕ at the scale of the domain height. At $\lambda = 1.0$ the flow is characterised by a continuously stratified surface layer deformed by turbulence in the outer boundary layer and diffuse overturns and elongated diffuse inclined structures. Small-scale overturns in ϕ are apparent throughout the core of the flow. The flow at $\lambda = 2.0$ has a similar character, but the near-surface region is almost completely inactive with no overturns in the temperature field.

In figure 5 the root-mean-square (r.m.s.) temperature fluctuation, $\langle\phi'\phi'\rangle^{1/2}$, is plotted normalised by $(I_s/\delta q_N)$. In the mixed region, $\langle\phi'\phi'\rangle^{1/2}$ is slightly larger at lower λ. The larger range of scales apparent in the near-wall region as seen in the flow visualisations in figure 4(*c*) also indicates this behaviour. In the thermocline, the increase in stability first increases the temperature fluctuations as turbulence is still active and works with an increased mean temperature gradient. At large stability for $\lambda = 0.2$–2.0, $\langle\phi'\phi'\rangle^{1/2}$ decreases near the free surface as turbulence is suppressed.

This structure contrasts with the numerous recent studies examining inhomogeneous stratified flow in a channel-type configuration (Komori *et al.* 1983; Garg *et al.* 2000; Armenio & Sarkar 2002; Nieuwstadt 2005; Taylor, Sarkar & Armenio 2005; Wang & Lu 2005; Deusebio *et al.* 2011; Flores & Riley 2011; Garcia-Villalba & del Alamo 2011; Zonta, Onorato & Soldati 2012) where N typically peaks at the walls.

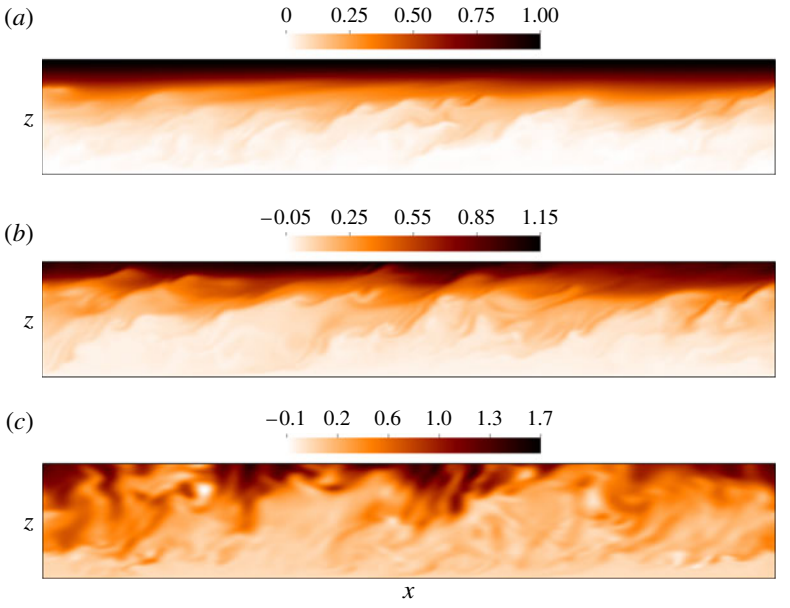

FIGURE 4. (Colour online) An instantaneous realisation of $(\phi - \phi_0)/\Delta\phi$ at $Re_\tau = 395$ and $\lambda = 2.0$ (a); $\lambda = 1.0$ (b); $\lambda = 0.1$ (c). Plot depicts full extent of domain, $L_x \times L_z = 2\pi \times \delta$.

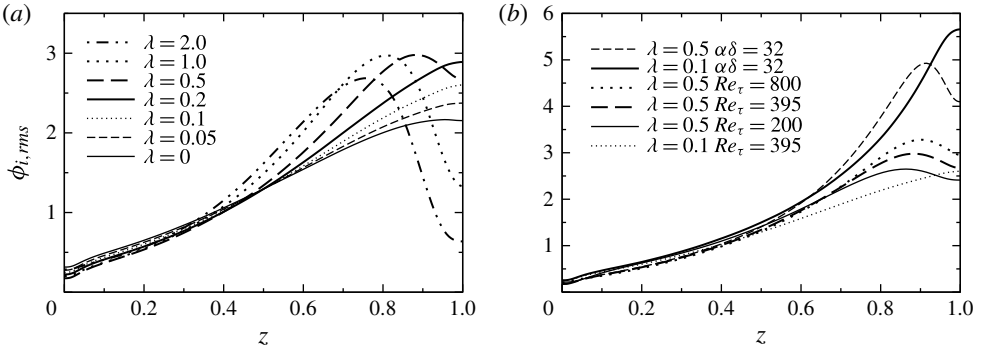

FIGURE 5. Temperature fluctuation normalised as $\langle\phi'\phi'\rangle^{1/2}/(I_s/\delta q_N)$ at $Re_\tau = 395$, $\alpha\delta = 8$ (a) and $Re_\tau = 200$–800, $\alpha\delta = 8$–32 (b).

Komori *et al.* (1983) performed experiments condensing steam in the free surface of an open channel. Garg *et al.* (2000) and Wang & Lu (2005) examined open channel flow with an isothermal surface and an adiabatic or isothermal lower boundary condition while Deusebio *et al.* (2011) examined the same configuration with constant fixed temperature difference across the channel. The canonical closed channel flow with a fixed temperature difference between the upper and lower walls was examined by Armenio & Sarkar (2002) and Garcia-Villalba & del Alamo (2011) in statistically steady conditions. These studies can be quantitatively related to our study by converting their $Ri_\tau = \Delta\rho g\delta/\rho_0 u_\tau^2$ to λ using $\lambda = (Nu/2)Ri_\tau/(PrRe_\tau)$ where Nu is the Nusselt number. Garcia-Villalba & del Alamo (2011) cover the range

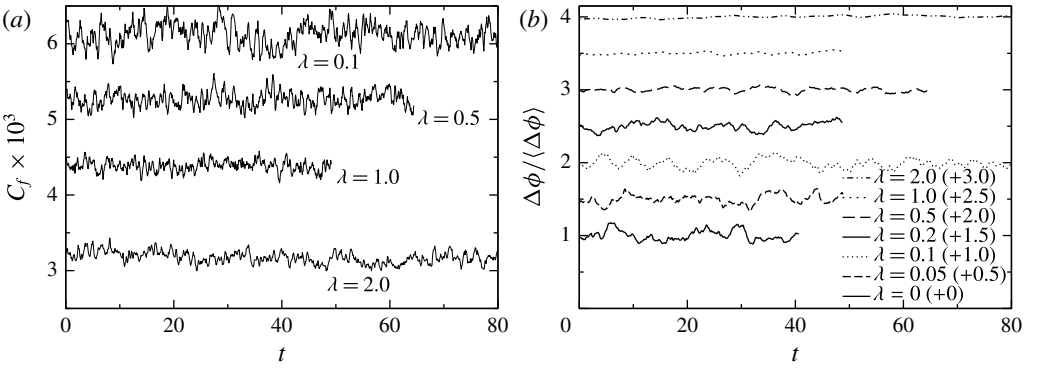

FIGURE 6. Variation of instantaneous bulk flow properties over non-dimensional flow time at $Re_\tau = 395$, $\alpha\delta = 8$: (*a*) skin friction $C_f = 2\langle u_\tau/u_b\rangle^2$ and (*b*) instantaneous plane-averaged temperature difference $\Delta\phi/\langle\Delta\phi\rangle + A$ where A is a vertical offset given in the figure.

$\lambda = 0$–3.4 at $Re_\tau = 180$–550 and $Pr = 0.7$ ($Ri_b = 0$–0.462), while Armenio & Sarkar (2002) covered $Ri_b = 0$–0.297 at $Re_\tau = 180$, $Pr = 0.71$ giving $\lambda = 0$–2.4.

Conditions more related to the present study were examined by Taylor *et al.* (2005), who used large-eddy simulation (LES) of an open channel flow with a constant heat flux at the upper stress-free boundary and an adiabatic lower wall with periodic spanwise and streamwise boundaries. Our configuration approaches this setting as $\alpha\delta \to \infty$. The results of Taylor *et al.* (2005) can be compared by converting their Ri_τ to λ using $\lambda = Ri_\tau/(2PrRe_\tau)$ and $E_r = \lambda\sqrt{C_f/2}$. They cover the range $Ri_b = 0$–0.118, $\lambda = 0$–0.125 and $E_r = 0$–6.8×10^{-3} at $Re_\tau = 400$ and $Pr = 5$, indicating that stratification is relatively weak.

There are also numerous studies of the atmospheric surface layer under stable conditions (e.g. Nieuwstadt 1984, 2005; Grachev *et al.* 2005; Wiel *et al.* 2008; Sorbjan & Grachev 2010; Flores & Riley 2011; Grachev *et al.* 2013). Unlike the stable atmospheric boundary layer, where $\langle b'w'\rangle$ and $\langle u'w'\rangle$ both decrease with height, in the present open channel configuration $\langle b'w'\rangle$ is zero at the wall and increases over most of the channel height and is non-monotonic. The inner wall region is then expected to be less susceptible to the transient re-laminarisation events that may be seen in these flows at low Reynolds number and high λ.

A consequence of our configuration is that we are able to attain statistically steady flow at relatively minimal domain sizes with regions of strong stratification present in the flow. The time-varying plane-averaged skin friction coefficient $C_f = 2\langle u_\tau/u_b\rangle^2$, is given in figure 6(*a*) for our $\lambda = 0.1$, 0.5, 1.0 simulations. The time variation in the plane-averaged $\Delta\phi$ normalised by time-averaged $\langle\Delta\phi\rangle$ is illustrated in figure 6(*b*) for $\lambda = 0$–2.0. In both the time trace of C_f and $\Delta\phi$ there is a range of long-time-scale oscillations of period $\Delta t \simeq 5$–10, longer than the turnover time $t = 1$ and the Brunt–Väisälä period $u_\tau/N\delta \lesssim 2$ for $\lambda = 0.05$. Similar observations were seen the closed channel flow of Garcia-Villalba & del Alamo (2011). In all cases here, however, the results converge to a statistically steady fully developed flow. The Reynolds number based on friction velocity computed directly from the flow field, u_τ^*, is displayed in table 1 as Re_τ^*. In all cases the result is within 0.1 % of the nominal Re_τ. This is in contrast to the stratified wall flow of Garcia-Villalba & del Alamo (2011) who found that much larger domain sizes were required in order to attain well-behaved statistically steady flow. The behaviour they observed was related to re-laminarisation

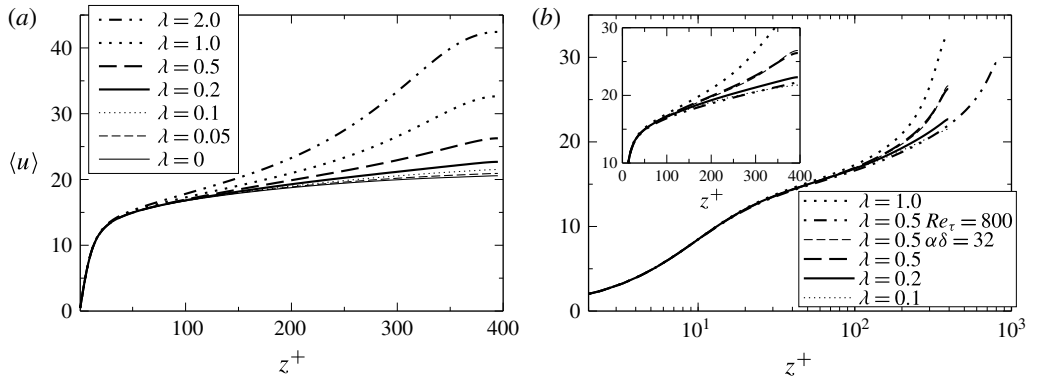

FIGURE 7. Variation of mean streamwise velocity profile u with height in wall units: (a) for $Re_\tau = 395$, $\alpha\delta = 8$ and $\lambda = 0$–2.0; and (b) $\alpha\delta = 8$–32.

at the wall and had a Reynolds number and λ dependence, so at $\lambda = 3.4$ and $Re_\tau = 550$, $(L_x, L_y) = (8\pi, 6\pi)$ was required. The present results at $Re_\tau = 395$ show no signs of re-laminarisation at the wall or divergence of the flow statistics in time with $(L_x, L_y) = (2\pi, \pi)$ up to our most stable case $\lambda = 2.0$.

In our $Re = 200$ tests we adopt initially a $(L_x, L_y) = (4\pi, 2\pi)$ domain to maintain the same size (L_x^+, L_y^+) in wall units. For $\lambda = 1.0$ at $Re_\tau = 200$ ($Re_{\mathscr{L}} = 200$), the flow had laminar streaks at the wall spanning the length of the domain and statistically steady conditions were not obtained. The domain size was increased to $(8\pi, 4\pi)$ and the flow remained turbulent across the entire wall region and a statistically steady fully developed solution was obtained. At $\lambda = 0.5$ at $Re_\tau = 200$ the laminar streaks or patches were not observed at $(4\pi, 2\pi)$.

With increasing stability λ, the skin friction coefficient, shown in table 1, decreases as the flow accelerates to a higher mean bulk velocity. The profile of the mean streamwise velocity is given in figure 7(a,b) with vertical location in wall units $z^+ = zu_\tau/\nu$. The velocity profiles illustrate that the inner boundary layer, $z^+ < 40$, is relatively unaffected, even at $\lambda = 2.0$ where there is approximately a factor of two increase in free-surface velocity compared with neutral flow. A clear separation of the velocity profiles only appears for $z^+ > 100$. This contrasts with the stratified wall flows of Armenio & Sarkar (2002); Garcia-Villalba & del Alamo (2011) where differences were clearly apparent in velocity and shear-stress profiles at $\lambda = 2$, $Re_\tau = 550$ (Garcia-Villalba & del Alamo 2011) and $\lambda = 1$, $Re_\tau = 180$ (Armenio & Sarkar 2002) at $z = 0.1$. In our $Re_\tau = 800$ result, the velocity profile lies close to the $\lambda = 0.1$, $Re_\tau = 395$ curve until $z^+ \simeq 350$, well into the outer layer. The influence of $\alpha\delta$ on the mean velocity profile appears to be relatively weak. In figure 7(b) the flow at $\lambda = 0.5$, $\alpha\delta = 32$ is nearly indistinguishable from the curve at $\alpha\delta = 8$. In figure 8(a,b), the shear stress $\langle u'w' \rangle$ is given for the same flows. As suggested by the velocity profiles, there is only slight variation from the neutral case over $z = 0$–0.3, while at $\lambda = 0.5$–2.0 the turbulent shear stress is significantly damped for $z > 0.6$ and at $\lambda = 2.0$ $\langle u'w' \rangle \simeq 0$ for $z > 0.9$.

In the statistically steady flow considered here the non-dimensional time-averaged temperature transport equation is

$$0 = -\frac{\mathrm{d}\langle w'\phi' \rangle}{\mathrm{d}z} + \frac{1}{Re_\tau Pr}\frac{\mathrm{d}^2\langle \phi \rangle}{\mathrm{d}z^2} + qe. \tag{3.1}$$

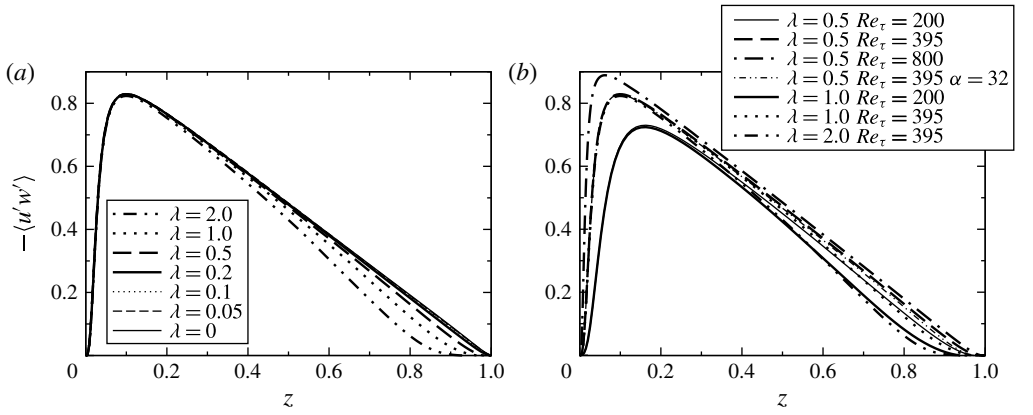

FIGURE 8. Turbulent shear stress, $-\langle u'w'\rangle$ at $Re_\tau = 395$, $\alpha\delta = 8$ (*a*) and $Re_\tau = 200$–800, $\alpha\delta = 8$–32 (*b*).

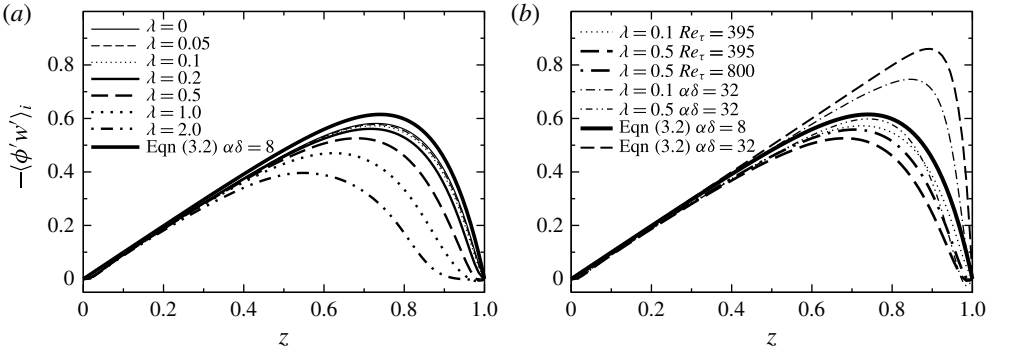

FIGURE 9. Scalar flux normalised as $-\langle\phi'w'\rangle/(I_s/\delta q_N)$ at $Re_\tau = 395$, $\alpha\delta = 8$ (*a*) and $Re_\tau = 395$–800, $\alpha\delta = 8$–32 (*b*).

In the laminar limit, it is expected that $\partial\phi/\partial z \sim PrRe_\tau I_s/\delta q_N$. These conditions are approached near the free surface at high λ, resulting in the increase in surface temperature at $\lambda = 0.5$ over $Re_\tau = 200$–800. In the limit of $1/Re_\tau Pr \to 0$ we can integrate over the channel height with the boundary condition $\langle\phi'w'\rangle = 0$ at $z = 0$ to obtain

$$-\langle\phi'w'\rangle/(I_s/\delta q_N) = \left(z - \mathrm{e}^{(z-1)\alpha\delta}\right). \tag{3.2}$$

Plotting this limit for $\alpha\delta = 8$–32 together with profiles of $-\langle\phi'w'\rangle$ in figure 9(*a*,*b*) reveals the extent to which the increased stability has reduced the turbulent heat flux. Over the mixed region the profiles $-\langle\phi'w'\rangle$ differ only slightly from (3.2), while through the thermocline the scalar flux is increasingly damped as suggested by the temperature profiles. Adjacent to the surface at $\lambda = 0.5$–2 a region exists where $-\langle\phi'w'\rangle < 0$ indicating counter-gradient heat transfer, as has been reported elsewhere in strongly stratified conditions (see Komori *et al.* 1983; Gerz, Schumann & Elghobashi 1989; Holt *et al.* 1992; Taylor *et al.* 2005).

It is clear that there is rapid variation in flow stability with z, allowing the influence of stratification to be examined within a single simulation flow field.

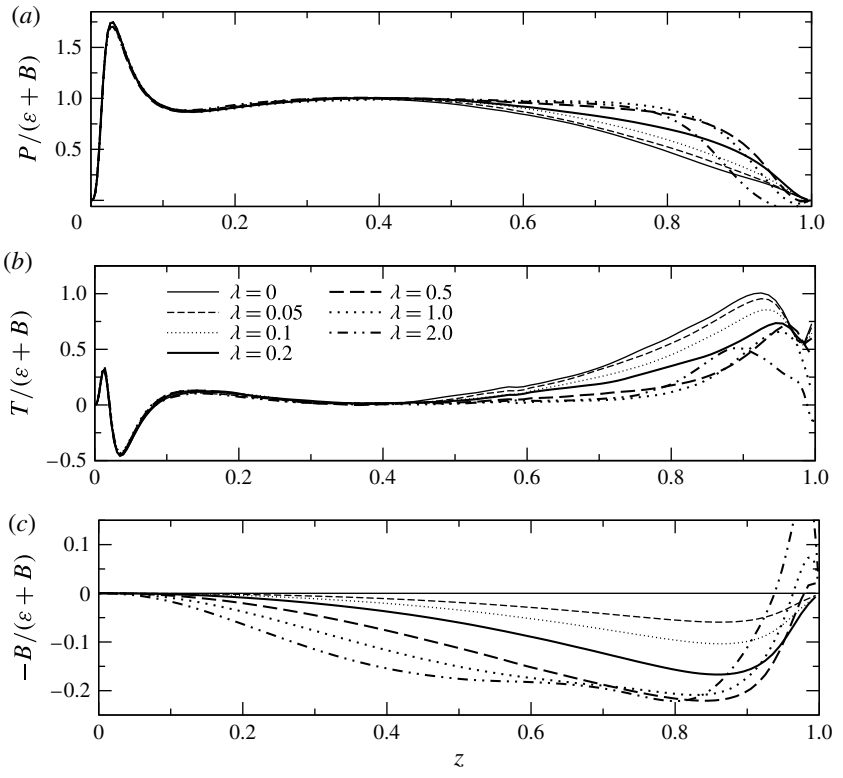

FIGURE 10. Turbulence kinetic energy transport terms as a ratio of total dissipation: (*a*) production $P/(\varepsilon+B)$, (*b*) turbulent diffusion $T/(\varepsilon+B)$ and (*c*) buoyancy flux $-B/(\varepsilon+B)$ or equivalently $-R_f$.

4. Transition to local energetic equilibrium and turbulence suppression

4.1. *Criterion for onset of strong stratification*

With the flow being statistically stationary and with homogeneity in the x–y plane, the TKE transport equations can be written in non-dimensional form as

$$\frac{\mathrm{d}}{\mathrm{d}z}\langle w'k\rangle + \frac{\mathrm{d}}{\mathrm{d}z}\langle w'p'\rangle - \frac{1}{Re_\tau}\frac{\mathrm{d}^2k}{\mathrm{d}z^2} = P-\varepsilon-B, \tag{4.1}$$

where the TKE is $k=0.5\langle u_i'u_i'\rangle$, the buoyancy flux $B=-\lambda\langle\phi'w'\rangle$, the turbulence dissipation rate $\varepsilon=(1/Re_\tau)\langle(\partial u_i'/\partial x_j)^2\rangle$ and the turbulence production term $P=-\langle u'w'\rangle\mathscr{S}$ where $\mathscr{S}=\mathrm{d}\langle u\rangle/\mathrm{d}z$. The transport terms on the left-hand side of (4.1) are the turbulent convection (T), pressure transport and viscous diffusion terms respectively. When the terms on the left-hand side are zero, the flow is in local equilibrium, with production and dissipation in balance, $P-\varepsilon-B=0$. The ratio of the dominant terms P, B and T to the total dissipation $\varepsilon+B$, are shown over the channel depth in figure 10.

At $\lambda=0$ a region of quasi-equilibrium where $P\simeq\varepsilon$ exists over $(50\lesssim z^+\lesssim 0.5Re_\tau)$. Above this region, the turbulent convection term increases and the outer layer is a net sink of turbulence. This compares well with experimental observation in neutral conditions in open channel flow (Komori *et al.* 1983; Nezu & Rodi 1986) and DNS

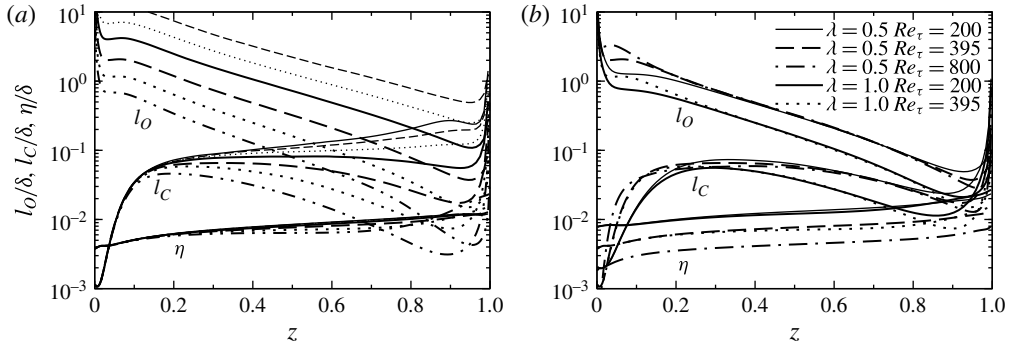

FIGURE 11. Variation of length scales l_O, l_C, η normalised by δ with z for (*a*) $\lambda = 0$–2.0 at $Re_\tau = 395$ with lines defined in figure 10; (*b*) $Re_\tau = 200$–800 and $\lambda = 0.5$–1.0.

of closed channel flow (Moser *et al.* 1999) over $Re_\tau = 395$–640. With increasing λ the equilibrium region, as indicated by $P/(\varepsilon + B) \sim 1$, extends further towards the free surface. At $\lambda = 0.5$–1.0, this equilibrium region extends to a near-surface region at $z \simeq 0.8$ above which there is a separate behaviour that we return to in § 6. Normalised in this form, the buoyancy flux is also known as the generalised flux Richardson number (Ivey & Imberger 1991),

$$R_f = \frac{B}{B + \varepsilon}, \tag{4.2}$$

which has observed limit values of $R_{f,c} \simeq 0.17$–0.25 (Ellison 1957; Osborn 1980; Ivey *et al.* 2008; Garcia-Villalba & del Alamo 2011). With increasing stability, R_f (figure 10*c*) rises to peak values in the region $z = 0.75$–0.85 where the scalar flux profile decreases rapidly with z (figure 9). At $\lambda = 2.0$ over $z = 0.5$–0.7 the flow approaches a local energetic mixing limit $R_{f,c} \simeq 0.18$.

This transition can also be seen in the length scales l_C and l_O which are shown in figure 11 with z together with the length scale η. With increasing buoyancy, l_C and l_O reduce, while η is relatively unaffected. The variation of the ratio of the outer length scales $Ri = (l_C/l_O)^{4/3}$ with z is shown in figure 12. In the near-wall region Ri rises from near-neutral values with height and with increasing flow stability. At $\lambda = 1.0$ between $z = 0.6$–0.77, Ri appears to asymptote to $Ri_c = 0.2$ before rising above this limit at $z = 0.77$. At $\lambda = 2.0$ the asymptote occurs over $z = 0.5$–0.77. The onset of limit conditions is similar to that observed for R_f. The relationship between the two parameters can be formed in equilibrium conditions from definitions as $Pr_t = Ri/R_f$ where the turbulent Prandtl number is

$$Pr_t = \frac{-\langle u'w' \rangle / \mathscr{S}}{B/\mathscr{N}^2} \tag{4.3}$$

and $\mathscr{N}^2 = \lambda \mathrm{d}\langle\phi\rangle/\mathrm{d}z$ is the non-dimensional Brunt–Väisälä frequency. The profiles of Pr_t in figure 13 show that, over the region $z < 0.6$, with increasing stability the flow increases from $Pr_t \simeq 0.8$ in neutral conditions to a nearly constant value of $Pr_t = 1.0$ at $\lambda = 2.0$.

It is clear that $\lambda \simeq 1$ represents a transition to local limit conditions for this flow in terms of $Pr_t \to 1$ and $P/(\varepsilon + B) \sim 1$ and that $Ri \to Ri_c$, $R_f \to R_{f,c}$ over an increasing portion of the boundary layer height with $\lambda > 1$.

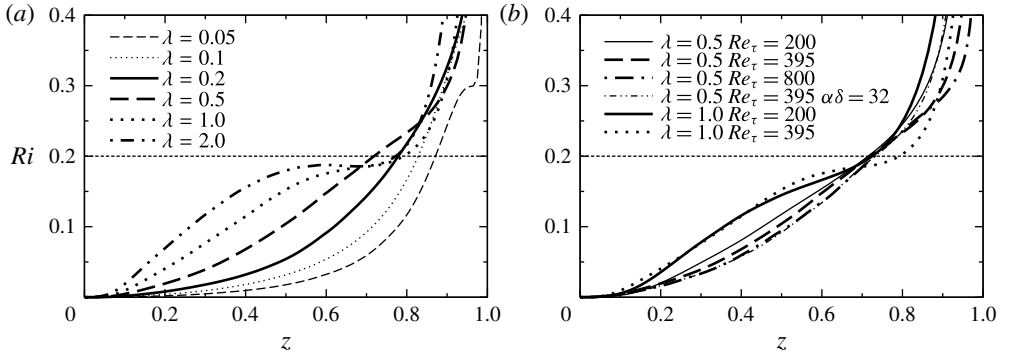

FIGURE 12. Variation of Ri with z for (*a*) $Re_\tau = 395$ with $\lambda = 0.05$–1.0 and (*b*) $Re_\tau =$ 200–800, $\alpha\delta = 8$–32 and $\lambda = 0.5$–1.0.

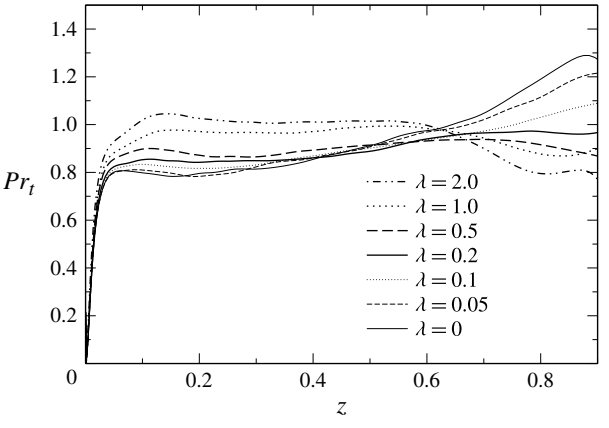

FIGURE 13. Pr_t for $\lambda = 0$–2.0.

4.2. $\mathscr{R}$ *affected regime*

With increasing stratification, l_O approaches the smallest scales of turbulent motion η. The ratio $\mathscr{R} = (l_O/\eta)^{4/3}$ is plotted in figure 14. The parameter varies over four orders of magnitude across the channel height. In the wall region $l_O \gg \eta$, indicating a wide separation between smallest scales and buoyancy affected scales, while with increasing z and λ this separation is reduced.

Recent discussion has identified this reduced separation of scales with the transition to a viscous regime of behaviour (Lindborg 2006; Brethouwer *et al.* 2007; Flores & Riley 2011; Chung & Matheou 2012). Shih *et al.* (2005) examined the mixing characteristics in homogeneous stratified shear flow and found that $\mathscr{R}_c \lesssim 7$ indicated transition to a molecular diffusive mixing regime. In a similar flow Brethouwer *et al.* (2007) showed that $\mathscr{R}_c = 1$ indicates the transition from a classic Kolmogorov energy cascade to a regime where vertical viscous shearing is important.

Applying these limits here suggests the low-$\mathscr{R}$ regime is attained over a part of the domain height for $\lambda \gtrsim 0.5$ at $Re_\tau = 395$. The limit $\mathscr{R}_c = 7$ intersects with the $\mathscr{R}$ profiles in figure 14(*a*) at $z = 0.9$, 0.8 and 0.7 for $\lambda = 0.5$, 1.0 and 2.0 respectively for $Re_\tau = 395$. The onset of a more suppressed regime of turbulent flow is also apparent in our mean flow statistics. In figure 10(*a*) the turbulence production term at $\lambda = 2$

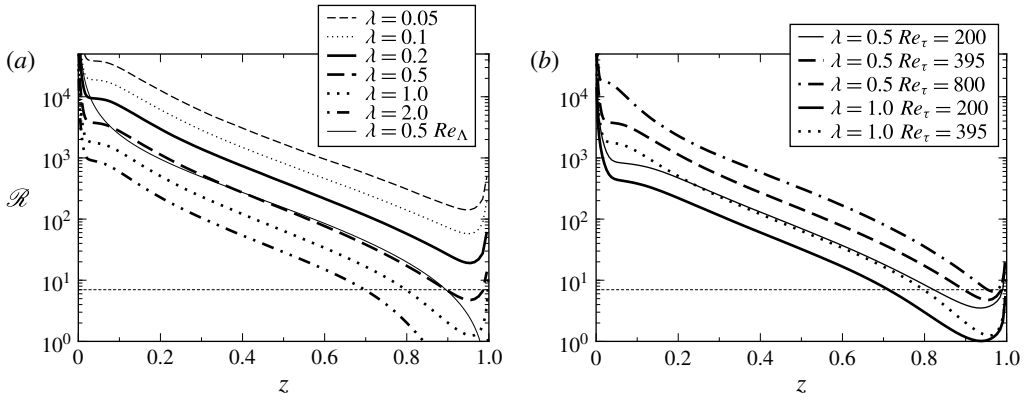

FIGURE 14. Variation of $\mathscr{R}$ with z at $Re_\tau = 395$ (*a*) and $Re_\tau = 200$–800 (*b*). In (*a*) the thin solid line indicates $\mathscr{R} = Re_\Lambda$ estimated from $Re_\Lambda = (1-z)^2 Re_\tau/\lambda(z - \mathrm{e}^{(z-1)\alpha\delta})$ at $Re_\tau = 395$ and $\lambda = 0.5$. Solid horizontal line indicates $\mathscr{R} = 7$.

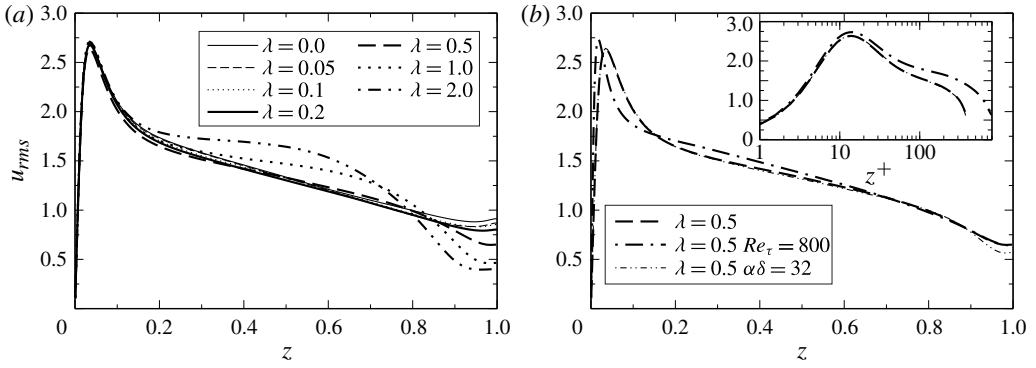

FIGURE 15. Streamwise r.m.s. velocity, $\langle u'u' \rangle^{1/2}$ at $Re_\tau = 395$, $\alpha\delta = 8$ (*a*) and $Re_\tau = 395$–800, $\alpha\delta = 8$–32 (*b*).

falls below the $\lambda = 1$ curve at $z \simeq 0.8$ while the $\lambda = 1$ curve falls below the $\lambda = 0.5$ curve at $z \simeq 0.9$. In figures 8 and 9 the shear stress and buoyancy flux are also reduced in these regions as are the buoyancy fluctuations in figure 5. The normal stresses are plotted in figures 15–17. In the neutral case our results are comparable with available data for open channel flow over $Re_\tau = 134$–1280 (Handler *et al.* 1993; Komori *et al.* 1993; Handler *et al.* 1999; Calmet & Magnaudet 2003; Nagaosa & Handler 2003). In stratified conditions, the wall-normal stress $\langle w'w' \rangle$ is suppressed with increasing λ for $z \simeq 0.4$. The horizontal stresses $\langle u'u' \rangle$ and $\langle v'v' \rangle$ are damped with increasing λ above $z \simeq 0.8$ but do not go to zero.

Studies of homogeneous sheared stratified turbulence have identified the onset of a regime of turbulence decay with an increase of Ri above Ri_c with $Ri_c = 0.2$–0.25 (Holt *et al.* 1992; Smyth & Moum 2000). The condition $Ri > Ri_c$ has also been shown to indicate the transient collapse in stable atmospheric boundary layer simulations (Nieuwstadt 2005) and field measurements (Grachev *et al.* 2013).

These Ri_c values correspond approximately to the high-λ asymptote identified in figure 12; however, in all simulations Ri increases to above Ri_c near the surface.

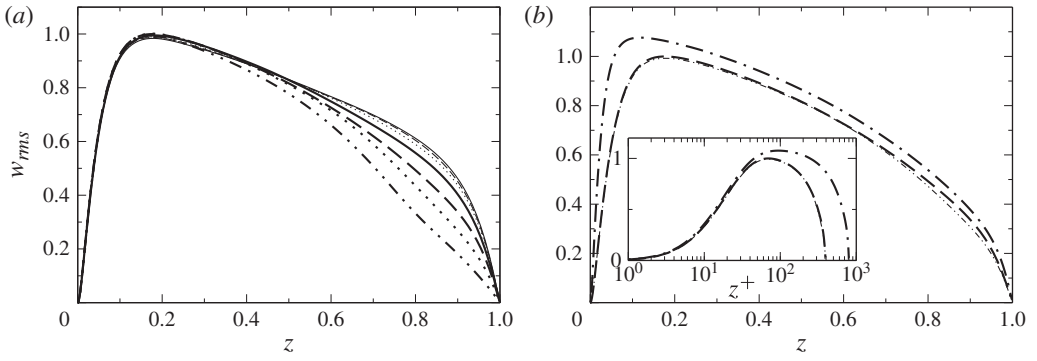

FIGURE 16. Wall-normal r.m.s. velocity, $\langle w'w' \rangle^{1/2}$ with lines defined in figure 15.

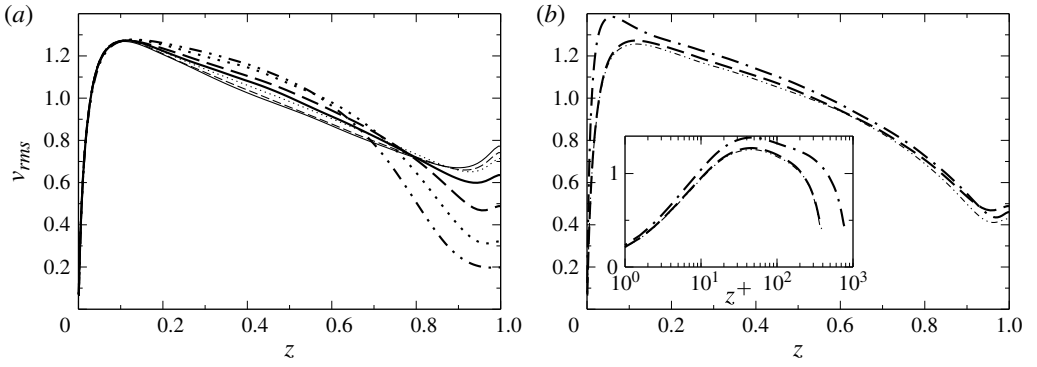

FIGURE 17. Spanwise r.m.s. velocity, $\langle v'v' \rangle^{1/2}$ with lines defined in figure 15.

At $\lambda = 0.1$, the turbulence intensities and shear stresses vary only slightly from neutral conditions so while $Ri > Ri_c$ at $z \simeq 0.8$ there is no evidence of turbulence collapse. In this way $Ri > Ri_c$ is not a sufficient condition for, or indication of, the transition to collapse of turbulence. This is also observed in the results of Garcia-Villalba & del Alamo (2011). Both our flow and the configuration of Garcia-Villalba & del Alamo (2011) are statistically stationary and inhomogeneous in z so turbulence can be transported vertically across the boundary layer from the region where $Ri < Ri_c$ to the outer more stable regions.

The behaviour of the gradient Richardson number at $\lambda = 0.5$ is counter-intuitive. Over $z = 0.7$–0.8 Ri is higher at $\lambda = 0.5$ than at $\lambda = 1.0$ and $\lambda = 2.0$, implying that at this location, an increase in buoyancy leads to less stable flow. This behaviour is also seen in the channel flow results of Garcia-Villalba & del Alamo (2011) between $\lambda = 0.54$ and $\lambda = 2.0$. The behaviour is apparently insensitive to Re_τ, as our $Re = 200$ and $Re = 800$ both have the same transition location to $Ri > Ri_c$ at $z \simeq 0.7$.

Comparing the $\mathscr{R}$ and Ri profiles and summarising our observations we can identify regimes of behaviour. For $\lambda = 0$–0.2, $\mathscr{R} \gg 7$ over the entire flow field and $Ri < Ri_c$ for $z < 0.75$. The flow is weakly affected by stratification with the turbulence intensities and fluxes $\langle u'w' \rangle$ and $\langle \phi'w' \rangle$ showing only slight variation from neutral conditions. For $\lambda \gtrsim 0.5$ local equilibrium behaviour is observed over the outer layer where $P/(\varepsilon + B) \sim 1$. Further increasing stability to $\lambda = 1.0$–2.0, R_f and Ri are observed to approach limit

values and $Pr_t \simeq 1.0$ over an extended region of the outer boundary layer. We found $Ri \simeq Ri_c$ and $\mathscr{R} > 7$ over $z = 0.5$–0.7 at $\lambda = 2$, while at $\lambda = 1.0$ these conditions are met over $z = 0.6$–0.77. Over these regions $\mathscr{R} \simeq 10$–40. The results of Shih *et al.* (2005) suggest that the flow in this regime is here is strongly stratified but outside the low $\mathscr{R} < 7$ regime. Similar behaviour is seen at $\lambda = 0.5$ at $Re_\tau = 200$ ($Re_{\mathscr{L}} = 400$).

In stratified wall flow, Flores & Riley (2011) identified L_* as a parameter indicating transient 'turbulence collapse' or re-laminarisation at the wall. Our $Re_{\mathscr{L}}$ parameter is equivalent to their parameter, differing only in the definition of the Obukhov length scale. Our configuration is quite different, however, and it is not immediately clear how $Re_{\mathscr{L}}$ identifies with the onset the molecular mixing regime, in localised regions of the flow field, when the near-wall region remains fully turbulent and at full development.

Since energetic equilibrium is attained before the onset of the diffusive regime, $Re_{\mathscr{L}}$ and Re_Λ can be directly interpreted in terms of $\mathscr{R}$. Using the energy balance approximation $P - \varepsilon - B = 0$, the local parameter $\mathscr{R}$ can be re-cast in terms of λ and R_f with $P/\varepsilon = 1/(1 - R_f)$ resulting in a non-dimensional form

$$\mathscr{R} \equiv \frac{\varepsilon Re_\tau}{\mathscr{N}^2} = \frac{\langle u'w' \rangle Re_\tau}{B} \frac{\varepsilon}{Pr_t \mathscr{S}} \simeq \frac{\langle u'w' \rangle^2 Re_\tau}{B} \frac{(1 - R_f)}{Pr_t} = Re_\Lambda \frac{(1 - R_f)}{Pr_t}. \tag{4.4}$$

In this way we have a local estimation of the buoyancy parameter $\mathscr{R} \simeq Re_\Lambda$ as $(1 - R_f)/Pr_t \simeq 1$ within the equilibrium region. Using the approximation $(1 - R_f)/Pr_t \simeq 1$, and the high-Reynolds-number approximations for the fluxes $\langle u'w' \rangle \simeq u_\tau^2(1 - z)$ and $\langle \phi'w' \rangle$, using (3.2) in (4.4) we can obtain the approximation $Re_\Lambda = (1 - z)^2 Re_{\mathscr{L}}/(z - \mathrm{e}^{(z-1)\alpha\delta})$, and which explicitly relates $\mathscr{R}$ to $Re_{\mathscr{L}}$. In figure 14(*a*) this estimate for Re_Λ at $\lambda = 0.5$ and $Re_\tau = 395$ is given, indicating reasonable agreement outside the near-wall and near-surface regions. There is also support for the $\mathscr{R} \sim Re_{\mathscr{L}}$ in figure 14(*b*), where flow at $\lambda = 0.5$, $Re_\tau = 200$ ($Re_{\mathscr{L}} = 400$), and flow at $\lambda = 1.0$, $Re_\tau = 395$ ($Re_{\mathscr{L}} = 395$) have approximately the same $\mathscr{R}$ profile over $0.3 < z < 0.8$.

If the onset of the diffusive regime can be identified with $\mathscr{R}$ it follows that the critical bulk parameter $Re_{\mathscr{L},c}$ can also be identified. The $\mathscr{R} = 7$ criterion suggests transition to a diffusive regime above $z \simeq 0.8$ when $Re_{\mathscr{L}} = 400$ or above $z \simeq 0.7$ when $Re_{\mathscr{L}} = 200$. Flores & Riley (2011) noted that their scaling L_* could be justified in terms of separation of largest ($\sim L$) and smallest ($\sim \nu/u_\tau$) scales in the dynamic sub-layer of a stratified boundary layer. Similarly, in the present context the $Re_{\mathscr{L}}$ term is related to separation of l_O and η in the outer boundary layer.

4.3. *Bulk parameters*

The $Re_{\mathscr{L}}$ transition is also visible through variation in the bulk Richardson number, $Ri_b = \Delta\phi\lambda\delta/u_b^2$, illustrated in figure 18, with λ, together with results of other channel flow studies in both open and closed configurations. Over $\lambda = 0.05$–1.0 and $\alpha\delta = 8$, our $Re_\tau = 200$ and $Re_\tau = 395$ results collapse to a single trend line with an empirical fit of $Ri_b \simeq 0.16\lambda^{4/3}$. At $Re_\tau = 200$, $\lambda = 1.0$ ($Re_{\mathscr{L}} = 200$) and $Re_\tau = 395$, $\lambda = 2.0$ ($Re_{\mathscr{L}} = 200$) the data points fall slightly below this curve. The DNS of Garcia-Villalba & del Alamo (2011) appear to asymptote to the same trend for $\lambda < 1$ in their $Re_\tau = 180$ and $Re_\tau = 550$ flows, notwithstanding the differences in configuration and Reynolds number. For $\lambda \gtrsim 1$ their data show that Ri_b increases with λ at a reduced rate with Reynolds number dependence. Their $Re_\tau = 180$ data appear to depart from our trend line at $\lambda \simeq 0.67$ ($Re_{\mathscr{L}} = 268$) while at $Re_\tau = 550$ the

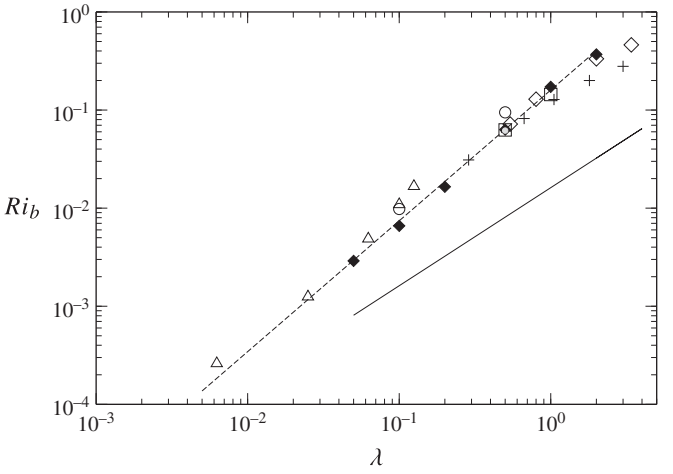

FIGURE 18. Variation of bulk parameter Ri_b with λ, where the symbols indicate $Pr = 0.7$–0.71 results: □, $Re_\tau = 200$; ◆, $Re_\tau = 395$; ●, $Re_\tau = 800$; ○, $\alpha\delta = 32$; +, Garcia-Villalba & del Alamo (2011) $Re_\tau = 180$; ◇, Garcia-Villalba & del Alamo (2011) $Re_\tau = 550$; △, Taylor *et al.* (2005) $Re_\tau = 400$, $Pr = 5.0$ result normalised to Ri_b (0.71/5.0). Lines are defined: – – – –, $Ri_b = 0.16\lambda^{4/3}$; ——, $Ri_b = 9\lambda Pr/Re_\tau$ with $Pr = 0.71$ and $Re_\tau = 395$.

departure occurs at $\lambda \simeq 2.0$ ($Re_{\mathscr{L}} = 278$) consistent with a transition to a molecular mixing regime dependent on $Re_{\mathscr{L},c}$.

We offer no explanation for the $Ri_b \sim \lambda^{4/3}$ trend but note that, in the laminar limit, turbulence is entirely suppressed so u_b is decoupled from the buoyancy field. In this case, the exact analytical result can be obtained. Taylor *et al.* (2005) showed that with $\alpha\delta \to \infty$, the dimensional density difference across the channel height is $\Delta\rho = |\mathrm{d}\rho/\mathrm{d}z|_s\delta/2$. In our setting this becomes $\Delta\rho = I_s\beta\delta/2\sigma C_p$. With $Ri_b = \Delta\rho g\delta/\rho u_b^2$ and $u_b/u_\tau = Re_\tau/3$ (Pope 2000) we obtain $Ri_b = 9\lambda Pr/Re_\tau$ as shown on figure 18. The reduced slope of our $Re_{\mathscr{L}} = 200$ simulations also suggests a transition to a more suppressed regime of scalar transport in agreement with the local observations, with the same critical limit as observed in § 4.2 of $Re_{\mathscr{L},c} \simeq 200$–$400$.

The comparison of the $Pr = 5.0$ result of Taylor *et al.* (2005) to the present $Pr = 0.71$ study is not straightforward. The temperature scale $\Delta\phi$ across their flow is set by the surface heat flux so $\mathrm{d}\langle\phi\rangle/\mathrm{d}z \sim Pr$. An approximate re-normalisation of their result is made here to our $Pr = 0.71$ values by $Ri_b \times 0.71/5.0$ as indicated in figure 18. Their results compare reasonably well apart from $\lambda > 0.1$ where, in their study, there is an increasingly thick diffusive region near the free surface, thereby increasing $\Delta\phi$ across the channel and hence Ri_b. Our $\alpha\delta = 32$ results behave in a similar manner.

In terms of E_r, the critical values for the onset of stratified conditions, in coastal flows $E_{r,c} \simeq 0.003$ and river channels 0.0044 (Bormans & Webster 1997), corresponds to $\lambda = 0.05$–0.1 in the present study, indicating near-neutral flow conditions. The bulk parameter E_r contains an additional Reynolds number dependence through skin friction coefficient variation in $E_r = \lambda(C_f/2)^{1/2}$, which is unrelated to the viscous parameter $Re_{\mathscr{L}}$. In our $\lambda = 0.5$ result across $Re_\tau = 200$–800 there is variation over $E_r = 0.023$–0.028 (in table 1) while the behaviour is apparently consistent in terms of the kinetic energy budgets and turbulence intensities and consistent in terms of bulk Ri_b behaviour. We note that in translating critical flow parameter values from flow in coastal seas, where Re is $O(10^7)$, to the smaller scale river flow considered

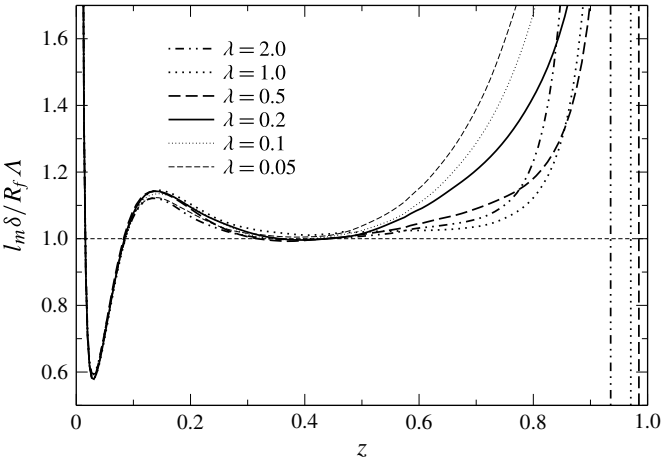

FIGURE 19. $l_m\delta/R_f\Lambda$ for $Re_\tau = 395$ with $\lambda = 0.05$–2.0.

in the present study, where Re is $O(10^5)$, the choice of parameter E_r or λ may lead to considerable variation in predicted behaviour.

4.4. *Parameterisation of turbulent mixing*

Transition behaviour can be viewed in terms of turbulent mixing. Recent studies (Osborn 1980; Shih *et al.* 2005; Ivey *et al.* 2008; Gonzalez-Juez *et al.* 2011; Chung & Matheou 2012) have suggested that the effects of buoyancy on turbulent mixing can be parameterised in terms of $\mathscr{R}$. For $\mathscr{R} < \mathscr{R}_c$ the mixing is reduced to molecular levels or $k_m \to 0$ (Shih *et al.* 2005). For $\mathscr{R} > \mathscr{R}_c$ Osborn (1980) showed $k_m \leqslant \epsilon/N^2$ or $k_m/\nu \simeq \Gamma\mathscr{R}$ where Γ is the mixing efficiency. At large $\mathscr{R}$ the dependence of k_m on $\mathscr{R}$ decreases (Shih *et al.* 2005) and ultimately becomes independent of $\mathscr{R}$ in neutral conditions (Chung & Matheou 2012).

The local mixing parameters can be re-cast in terms of λ and R_f. The non-dimensional mixing length

$$l_m = \langle u'w'\rangle^{1/2}/S \tag{4.5}$$

can be normalised with the $P - \varepsilon - B = 0$ approximation to

$$\frac{l_m}{R_f(\Lambda/\delta)} \simeq \frac{B+\varepsilon}{P} \simeq 1.0. \tag{4.6}$$

This ratio, presented in figure 19, effectively demonstrates the range where local equilibrium holds. When $R_f \simeq R_{f,c}$, then $l_m \sim \Lambda/\delta$, consistent with limit conditions in Monin–Obukhov similarity models (Businger *et al.* 1971; Chung & Matheou 2012). Garcia-Villalba & del Alamo (2011) showed that the local Obukhov length scale can be used to scale features of the turbulent two-dimensional velocity spectra in channel flow for $\kappa z/\Lambda \gtrsim 1$, also consistent with our bulk parameter range for equilibrium $\lambda = \delta/\mathscr{L} \gtrsim 1.0$. The transition in mixing behaviour can also be seen in terms of the eddy viscosity ratio k_m/ν,

$$k_m/\nu \equiv \langle u'w'\rangle Re_\tau/S = Pr_t B Re_\tau/\mathscr{N}^2 \simeq Pr_t\Gamma\mathscr{R} = R_f Re_\Lambda, \tag{4.7}$$

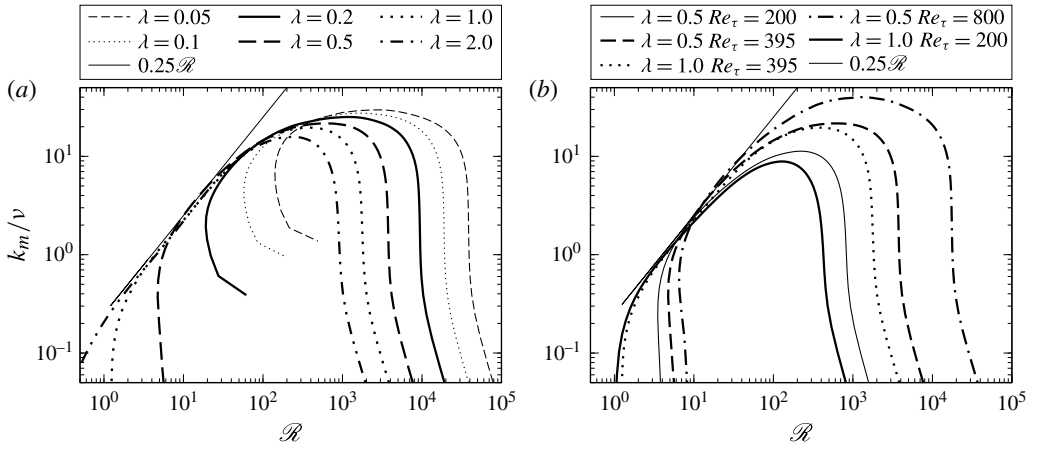

FIGURE 20. Variation of eddy viscosity ratio, k_m/ν, with $\mathscr{R}$ at $Re_\tau = 395$ (a) and $Re_\tau =$ 200–800 (b). Straight solid line indicates $k_m/\nu = 0.25\mathscr{R}$.

where the mixing efficiency is given as $\Gamma = B/\varepsilon \equiv R_f/(1 - R_f)$. Vertical profiles of k_m/ν are given in figure 20 versus local values of $\mathscr{R}$. The transition behaviour seen here through a sweep across the boundary layer height has the same behaviour as observed in the single-parameter-set simulations in homogeneous stratified shear flow of Shih *et al.* (2005) and Chung & Matheou (2012). The $Re_\tau = 395$ results appear to asymptote to $k_m/\nu = 0.25\mathscr{R}$ at $\mathscr{R} \simeq 30$ while those at $Re_\tau = 800$ and $Re_\tau =$ 200 transition at $\mathscr{R} = 60$ and $\mathscr{R} = 10$–20. At higher $\mathscr{R}$ the flow approaches neutral behaviour with k_m/ν independent of $\mathscr{R}$. There is an extended transition over $\mathscr{R}$ of $O(10)$ between these limits. In the small-$\mathscr{R}$ limit, the asymptote $0.25\mathscr{R}$ indicates $\mathscr{R} =$ 4 as a limit for $k_m/\nu \simeq 1$ in line with the $\mathscr{R} = 7$ value given by Shih *et al.* (2005).

5. Near-wall flow

In the near-wall region we have observed $Ri \ll Ri_c$ and $\mathscr{R} \gg 7$, indicating only weakly stratified flow with wide separation of viscous and buoyancy scales, an observation reinforced by the very slight variation in the velocity profile, shear stress, normal stresses (figures 15–17) and TKE budget within this region with increasing λ. We can quantify this sensitivity (or lack thereof) more precisely by examining the scaling for the near-wall velocity profiles in the near-wall region with λ and Re_τ.

The relation $\gamma = z^+ \mathrm{d}u/\mathrm{d}z^+$ is shown in figure 21 with vertical location in wall units. In a log-law region γ should be a constant $1/\kappa \simeq 2.44$ in neutral flow. The profiles correspond across the range of Reynolds numbers and λ for $z^+ < 30$, within the viscous region, but there is rapid divergence with both quantities above this height. In the neutral case $\gamma \simeq 2.5$ over $z^+ = 50$–75, which is somewhat higher than the closed channel flow $Re_\tau = 392$ result of Moser *et al.* (1999) but suggests a short region where the log law holds. In the stratified flows there is a consistent increase in γ with λ for $z^+ > 30$. It is clear from figure 21 that the inner wall region is influenced by stratification, albeit significantly less than in previous stratified wall studies such as Garcia-Villalba & del Alamo (2011) as suggested by their observed near-wall re-laminarisation events and larger near-wall buoyancy flux.

The $\lambda = 0.5$ result at $Re_\tau = 800$ lies between the $\lambda = 0$ and 0.1 results at $Re_\tau = 395$ out to $z^+ \simeq 200$, considerably lower than the $\lambda = 0.5$ result at $Re_\tau = 395$. At the

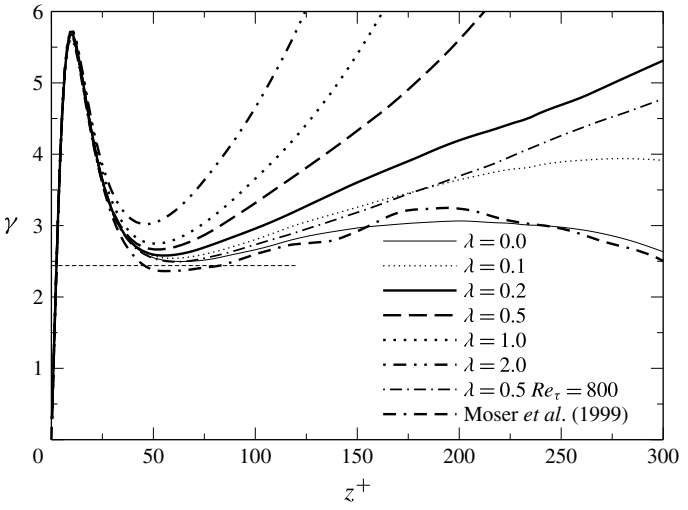

FIGURE 21. Log-law constant, $\gamma = z^+ \mathrm{d}u/\mathrm{d}z^+$. Thin horizontal line indicates $1/\kappa = 2.44$. Closed channel flow data of Moser *et al.* (1999) at $Re = 392$ indicated for comparison.

Reynolds numbers used here, there are expected to be low-Reynolds-number effects leading to variation in γ even in the neutral case (Moser *et al.* 1999); however, the greater part of this variation is due to the differing near-wall scaling of the shear stress and buoyancy flux profiles. The buoyancy flux $B = -\lambda\langle\phi' w'\rangle$ profile varies with z expressed in outer layer units, while by definition the beginning of the apparent log-law behaviour at $z^+ \simeq 50$ scales with viscous wall units ($z^+ = zRe_\tau$). Over the near-wall region there is a near linear decrease in B to $z = 0$, $B = 0$ (figure 9), so at fixed z^+, B is inversely proportional to Reynolds number.

This Reynolds number influence can also be seen in the scaling for $\mathscr{R}$ profiles in the near-wall region. We obtain the scaling $\mathscr{R} \sim Re_\Lambda$ from (4.4), which holds where there is energetic equilibrium, including the log-law region as shown in figure 10(*a*). From definitions in (1.7*b*) and (1.10*b*) we can write in non-dimensional form $Re_\Lambda(z) = -\langle u'w'\rangle^2 Re_\tau/\lambda\langle\phi' w'\rangle$ and re-arrange to obtain $Re_\Lambda(z) = -Re_{\mathscr{L}}\langle u'w'\rangle^2/\langle\phi' w'\rangle$. In the lower log-law region, say at $z^+ = 50$, $\langle u'w'\rangle \simeq u_\tau \simeq 1$ while the buoyancy flux $-\langle\phi' w'\rangle \simeq z(I_s/\delta q_N)$ from (3.2). In wall units then $-\langle\phi' w'\rangle \simeq z^+(I_s/\delta q_N)/Re_\tau$ so $Re_\Lambda(z^+) \sim Re_{\mathscr{L}} Re_\tau/z^+(I_s/\delta q_N)$ and $\mathscr{R} \sim Re_{\mathscr{L}} Re_\tau$.

This sensitivity is apparent in the $\mathscr{R}$ profiles for $\lambda = 0.5$ in figure 14(*b*). At $z = 0.05$, at $Re_\tau = 200$, $\mathscr{R} \simeq 825$, at $Re_\tau = 395$, $\mathscr{R} \simeq 3636$ and at $Re_\tau = 800$, $\mathscr{R} \simeq 13\,937$, giving a factor of 4.4 and 3.8 between these values, approximately in line with this scaling. The $\lambda = 1.0$, $Re_\tau = 395$ ($Re_{\mathscr{L}} = 395$) and $\lambda = 0.5$, $Re_\tau = 200$ ($Re_{\mathscr{L}} = 400$) cases converge at $z \simeq 0.3$ suggesting the limit of this behaviour in line with the outer extent of the log-law region in high-Reynolds-number neutral flow (Pope 2000). Similar sensitivity is also seen in the γ profiles in the near-wall region. The profile of γ at $\lambda = 0.5$, $Re_\tau = 800$ is close to that at $\lambda = 0.1$ for $Re_\tau = 395$, suggesting that halving of Re_τ is equivalent to approximately a five-fold increase in λ.

This scaling contrasts with stratified wall flows where $-\langle\phi' w'\rangle \simeq (I_s/\delta q_N)$, that is with no z dependence in the outer layer, so $\mathscr{R} \sim Re_{\mathscr{L}}$.

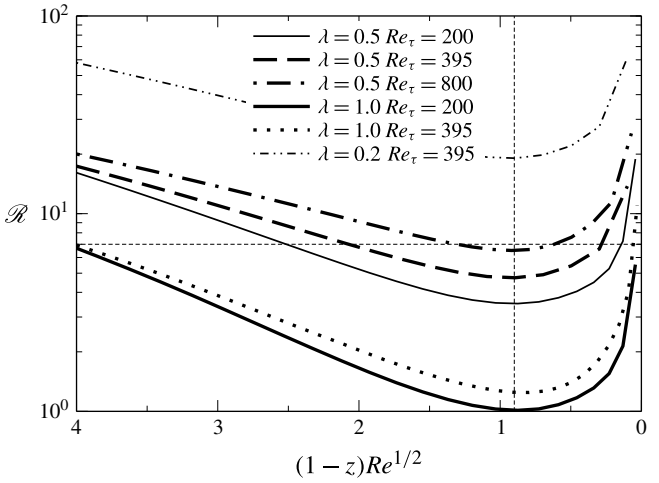

FIGURE 22. Variation of near-surface profiles of $\mathscr{R}$ with $(1-z)Re^{1/2}$ with vertical line indicating $(1-z)Re^{1/2} = 0.9$.

6. Scaling for free-surface affected region

In neutral conditions, the free surface affects the flow structure over a distance related to the integral length scale, l_∞, below the surface (Hunt & Graham 1978; Calmet & Magnaudet 2003). Calmet & Magnaudet (2003) estimated $l_\infty/\delta \sim 0.2$ and showed that this region coincides with the diverging near-surface profiles of u_{rms} and w_{rms}. In our neutral flow results, the wall-normal turbulent intensity shown in figure 16(*a*), decreases at a faster rate above $z \simeq 0.8$, indicative of this region.

Hunt & Graham (1978) treated this region as a 'source layer', which supplied turbulence to an inner viscous sub-layer. This inner layer is characterised by a length scale l_ν, which has the scaling $l_\nu/l_\infty = O(Re_\infty^{-1/2})$, where the Reynolds number can be defined $Re_\infty = l_\infty u/\nu$ (Hunt & Graham 1978; Hunt 1984; Calmet & Magnaudet 2003). Calmet & Magnaudet (2003) showed that the velocity scale can be taken as the wall friction velocity since the magnitude of the turbulence intensity at the surface is relatively insensitive to Reynolds number and is $O(u_\tau)$. This is seen in our neutral flow results where the streamwise turbulence intensity at the surface has a value of $\langle uu' \rangle^{1/2} = 0.91$, the same as found by Calmet & Magnaudet (2003) at $Re_\tau = 1280$, and close to $u_\tau = 1$.

The Reynolds number sensitivity is suggested in the spanwise and streamwise turbulence intensity profiles of our neutral flow results shown in figures 15(*a*) and 17(*a*). The spanwise stress $\langle v'v' \rangle^{1/2}$ reaches a minimum value at $z = 0.9$ while Calmet & Magnaudet (2003) reported $z = 0.925$ at $Re_\tau = 1280$ and Handler *et al.* (1999) $z = 0.83$–0.9 at $Re_\tau = 180$.

The Reynolds number dependence appears to be maintained even at high levels of stratification. At $\lambda = 0.5$, the intensity $\langle v'v' \rangle^{1/2}$ reaches minimum near-surface values at $z = 0.938$, 0.955 and 0.968 at $Re_\tau = 200$, $Re_\tau = 395$ and $Re_\tau = 800$ respectively. There is also little variation in the magnitude of intensities through the near-surface region with Reynolds number, with the surface values of $\langle u'u' \rangle^{1/2}$ being 0.65 and 0.66 at $Re_\tau = 395$ and 800 respectively.

Calmet & Magnaudet (2003) found $l_\nu \simeq 2Re_\infty^{-1/2} l_\infty$, determined by locating the near-surface peak in r.m.s. vorticity. Taking the integral length scale to be $l_\infty/\delta \sim 0.2$ and

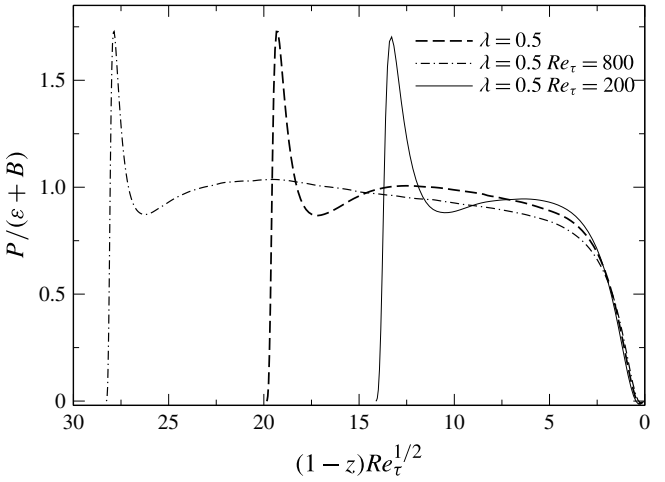

FIGURE 23. Turbulent kinetic energy production as a ratio of total dissipation $P/(\varepsilon + B)$ at $Re_\tau = 200$–800, with location from free surface $(1-z)$ normalised by $Re_\tau^{1/2}$.

$Re_\infty = Re_\tau l_\infty/\delta$, this scaling indicates $l_\nu/\delta \simeq 0.04$ at $Re_\tau = 395$. We examine the near-surface behaviour of our results using the $\mathscr{R}$ profiles in figure 22. We have scaled the near-surface distance $(1-z)$ with $Re^{1/2}$. In all the data sets shown, there is a location of minimum $\mathscr{R}$ just below the surface which appears to scale to $(1-z)Re^{1/2} = 0.9$. For $Re_\tau = 395$ this location gives $(1-z) = 0.045$, approximately the same as the $l_\nu/\delta \simeq 0.04$ estimate.

This Reynolds number influence can also be seen in the energy balance ratio $P/(\varepsilon + B)$ plotted in figure 23(*a*). Here we show results at $\lambda = 0.5$ over the Reynolds number range $Re_\tau = 200$–800. The near-surface $(1-z)Re_\tau^{1/2}$ scaling appears to collapse the three curves over $(1-z)Re_\tau^{1/2} \simeq 0$–2. This corresponds to $(1-z) \simeq 0.1$ at $Re_\tau = 395$, approximately twice the estimated l_ν in neutral flow, suggesting a wider length over which the l_ν scaling is relevant.

Calmet & Magnaudet (2003) argued that the evolution of near-surface vorticity can be related to the Taylor micro-scale l_t, noting that $l_t/l_\infty \sim Re_\infty^{-1/2}$, the same as the l_ν/l_∞ scaling of Hunt & Graham (1978). We can consider the effect of buoyancy on the near-surface l_ν scaling through extension of these Taylor micro-scale arguments. Using dimensional variables, the Taylor micro-scale is defined $l_t^2 = \nu\langle u^2\rangle/\epsilon$, where ϵ is the dimensional dissipation rate of TKE. The neutral flow turbulence intensities and the dissipation rate are nearly constant with Reynolds number in the near-surface region. In stratified flow, however, ϵ will vary. In stratified flow we can relate the buoyancy flux to the dissipation rate with the definition of mixing efficiency, $\epsilon = \langle b'w'\rangle/\Gamma$, to obtain $l_t^2 = \nu\langle u^2\rangle\Gamma/\langle b'w'\rangle$.

If we adopt u_{rms} as the velocity scale, and note from figure 15(*a*) that at the approximate boundary of the source layer $z \simeq 0.8$, $u_{rms}/u_\tau \simeq 1$, we obtain $l_t^2 \simeq \nu\Gamma u_\tau^2/\langle b'w'\rangle$. We can use the relations $\Lambda = \langle u'w'\rangle^{3/2}/\langle b'w'\rangle$ and $u_\tau^2 \simeq \langle u'w'\rangle$ to obtain $l_t^2 \simeq \nu\Gamma\Lambda/u_\tau$. Here we are essentially arguing that the flow near the surface is characterised by the properties of the turbulence, transported into the source layer from the stratified boundary layer, at $z \simeq 0.8$.

In non-dimensional form this becomes $l_t^2/\delta^2 \simeq \Gamma\Lambda/\delta Re_\tau$. The local Obukhov length scales with $\Lambda/\delta \sim 1/\lambda$ so we can obtain the scaling $l_t/\delta \sim \Gamma^{1/2}(Re_\tau\lambda)^{-1/2}$. In this

relationship Γ is an unknown property of the turbulence. In very stable flow, however, limit conditions are approached. In figure 10(*c*) we have seen that $R_f \to R_{f,c}$ at $z \simeq 0.8$ for $\lambda \gtrsim 0.5$. This implies $\Gamma \to \Gamma_c$ under strong stable conditions so the scaling can be reduced to $l_t/\delta \sim (Re_\tau \lambda)^{-1/2}$.

It is clear that in the inner layer the $\mathscr{R}$ behaviour does not have this character in figure 22 but we note that in the spanwise turbulence intensity profile shown in figure 17(*a*) there is a location in the surface region where intensity $\mathrm{d}\langle v'v'\rangle/\mathrm{d}z = 0$ and that this location has a λ sensitivity, particularly for $\lambda = 0.05$–0.2. In these cases, however, Γ is varying significantly with λ and z at $z \simeq 0.8$ (see R_f in figure 10*c*) making any comparison unsatisfactory. For $\lambda \geqslant 1.0$, $\mathscr{R} < \mathscr{R}_c$ near $z \simeq 0.8$ signifying the onset of the diffusive regime.

In summary we are not able to report convincing evidence for the λ sensitivity of this scaling but can report that the Reynolds number dependence is maintained in the same way as seen in neutral flow.

7. Conclusions

We have examined turbulent stratified open channel flow. Our buoyancy bulk parameter is defined through the ratio of the domain height δ to $\mathscr{L}$, denoted λ, a bulk Obukhov length scale for the flow, covering the range $\delta/\mathscr{L} = 0$–2.0 at $Re_\tau = 395$. We obtain a boundary layer flow where the effects of stratification are weak in the near-wall region but progressively stronger in the outer layer up to the free surface.

With increasing flow stability, two significant changes occur in the flow. Firstly the flow becomes local for $\lambda \gtrsim 0.5$, with turbulence production and dissipation in local equilibrium, $P/(\varepsilon + B) \sim 1$, extending from the near-wall region, $z^+ > 50$, to a near-surface limit, which we find is characterised by the same near-surface scaling as in neutral flow. For fixed $\lambda = 0.5$ this length is $(1-z)Re_\tau^{1/2} \simeq 2$. In this equilibrium region the flow can be characterised in terms of the flux Richardson number R_f and the local Obukhov length scale Λ; for example, a mixing length can be defined as $l_m \simeq R_f \Lambda/\delta$. Above $\lambda \simeq 1.0$, limit values for flux Richardson number $R_f = R_{f,c} \simeq 0.17$–$0.2$ and $Ri = Ri_c \simeq 0.2$ are obtained over a fraction of the channel height. We find that the critical buoyancy parameter $E_{r,c}$ is not as general as λ as it contains a Reynolds number dependence in C_f.

At higher λ we obtain a flow field where buoyancy interacts with the smallest scales of motion. We find that this regime can be identified by the parameter $Re_{\mathscr{L},c} = \mathscr{L} u_\tau/\nu \lesssim 200$–$400$, which is related to the L_* parameter of Flores & Riley (2011). In the energetic equilibrium, the local buoyancy Reynolds number $Re_\Lambda = \Lambda u_\tau/\nu$ is related directly to the separation of l_O and η in the outer boundary layer by $Re_\Lambda \simeq \mathscr{R} \equiv (l_O/\eta)^{4/3}$. We observed that a consequence of the inhomogeneity of this flow appears to be that regions of $Ri \gg Ri_c$ are obtained where the flow is turbulent and $\mathscr{R} \gg \mathscr{R}_c$.

An interesting feature of this configuration is that statistically steady flow can be attained in relatively small computational domain sizes, unlike previously reported stratified boundary layer flows. The apparent difference here is that the near-wall region appears only subtly affected by stratification with $\mathscr{R} \sim Re_{\mathscr{L}} Re_\tau$, in contrast to flows where buoyancy flux is non-zero at the wall and $\mathscr{R} \sim Re_{\mathscr{L}}$.

Acknowledgements

The authors gratefully acknowledge the support of the Australian Research Council (ARC). The first author was supported by ARC Post-doctoral Research Fellowship DP110103417.

REFERENCES

ABE, H., KAWAMURA, H. & MATSUO, Y. 2001 Direct numerical simulation of a fully developed turbulent channel flow with respect to Reynolds number dependence. *Trans. ASME: J. Fluids Engng* **123**, 382–393.

ARMENIO, V. & SARKAR, S. 2002 An investigation of stably stratified turbulent channel flow using large-eddy simulation. *J. Fluid Mech.* **459**, 1–42.

ARMFIELD, S. W., NORRIS, S. E., MORGAN, P. & STREET, R. 2002 A parallel non-staggered Navier–Stokes solver implemented on a workstation cluster. In *Proceedings of the Second International Conference on Computational Fluid Dynamics* (ed. S. Armfield, P. Morgan & K. Srinivas), pp. 30–45. Springer.

BARRY, M. E., IVEY, G. N., WINTERS, K. B. & IMBERGER, J. 2001 Measurements of diapycnal diffusivities in stratified fluids. *J. Fluid Mech.* **442**, 267–291.

BORMANS, M. & WEBSTER, I. T. 1997 A mixing criterion for turbid rivers. *Environ. Model. Softw. Environ. Data News* **12** (4), 329–333.

BRETHOUWER, G., BILLANT, P., LINDBORG, E. & CHOMAZ, J.-M. 2007 Scaling analysis and simulation of strongly stratified turbulent flows. *J. Fluid Mech.* **585**, 343–368.

BUSINGER, J. A., WYNGAARD, J. C., IZUMI, Y. & BRADLEY, E. F. 1971 Flux-profile relationships in the atmospheric surface layer. *J. Atmos. Sci.* **28**, 181–189.

CALMET, I. & MAGNAUDET, J. 2003 Statistical structure of high-Reynolds-number turbulence close to the free surface of an open-channel flow. *J. Fluid Mech.* **474**, 355–378.

CHUNG, D. & MATHEOU, G. 2012 Direct numerical simulation of stationary homogeneous stratified sheared turbulence. *J. Fluid Mech.* **696**, 434–467.

DEUSEBIO, E., SCHLATTER, P., BRETHOUWER, G. & LINDBORG, E. 2011 Direct numerical simulations of stratified open channel flows. *J. Phys. Conf. Ser.* **318**, 022009.

DILLON, T. M. & CALDWELL, D. R. 1980 The Batchelor spectrum and dissipation in the upper ocean. *J. Geophys. Res.* **85** (C4), 1910–1916.

ELLISON, T. H. 1957 Turbulent transport of heat and momentum from an infinite rough plane. *J. Fluid Mech.* **2**, 456–466.

FLORES, O. & RILEY, J. J. 2011 Analysis of turbulence collapse in the stably stratified surface layer using direct numerical simulation. *Boundary-Layer Meteorol.* **139** (2), 241–259.

GARCIA-VILLALBA, M. & DEL ALAMO, J. C. 2011 Turbulence modification by stable stratification in channel flow. *Phys. Fluids* **23** (4), 045104.

GARG, R. P., FERZIGER, J. H., MONISMITH, S. G. & KOSEFF, J. R. 2000 Stably stratified turbulent channel flows. I. Stratification regimes and turbulence suppression mechanism. *Phys. Fluids* **12** (10), 2569–2594.

GARGETT, A. E., OSBORN, T. R. & NASMYTH, P. W. 1984 Local isotropy and the decay of turbulence in a stratified fluid. *J. Fluid Mech.* **144**, 231–280.

GARRETT, C. J. R., KEELEY, J. R. & GREENBERG, D. A. 1978 Tidal mixing versus thermal stratification in the Bay of Fundy and Gulf of Maine. *Atmos.-Ocean* **16** (4), 403–423.

GERZ, T., SCHUMANN, U. & ELGHOBASHI, S. E. 1989 Direct numerical simulation of stratified homogeneous turbulent shear flows. *J. Fluid Mech.* **200**, 563–594.

GONZALEZ-JUEZ, E. D., KERSTEIN, A. R. & SHIH, L. H. 2011 Vertical mixing in homogeneous sheared stratified turbulence: a one-dimensional-turbulence study. *Phys. Fluids* **23** (5), 055106.

GRACHEV, A. A., ANDREAS, E. L., FAIRALL, C. W., GUEST, P. S. & PERSSON, P. O. G. 2013 The critical Richardson number and limits of applicability of local similarity theory in the stable boundary layer. *Boundary-Layer Meteorol.* **147** (1), 51–82.

GRACHEV, A. A., FAIRALL, C. W., PERSSON, P. O. G., ANDREAS, E. L. & GUEST, P. S. 2005 Stable boundary-layer scaling regimes: the SHEBA data. *Boundary-Layer Meteorol.* **116** (2), 201–235.

HANDLER, R. A., SAYLOR, J. R., LEIGHTON, R. I. & ROVELSTAD, A. L. 1999 Transport of a passive scalar at a shear-free boundary in fully developed turbulent open channel flow. *Phys. Fluids* **11**, 2607–2625.

HANDLER, R. A., SWEAN, T. F., LEIGHTON, R. I. & SWEARINGEN, J. D. 1993 Length scales and the energy balance for turbulence near a free surface. *AIAA J.* **31** (11), 1998–2007.

HEARN, C. J. 1985 On the value of the mixing efficiency in the Simpson-Hunter h/u^3 criterion. *Dtsch. Hydrogr. Z.* **38** (3), 133–145.

HOLLOWAY, P. E. 1980 A criterion for thermal stratification in a wind-mixed system. *J. Phys. Oceanogr.* **10**, 861–869.

HOLT, S. E., KOSEFF, J. R. & FERZIGER, J. H. 1992 A numerical study of the evolution and structure of homogeneous stably stratified sheared turbulence. *J. Fluid Mech.* **237**, 499–539.

HUNT, J. C. R. 1984 Turbulence structure and turbulent diffusion near gas–liquid interfaces. In *Gas Transfer at Water Surfaces* (ed. W. Brutseart & G. H. Jirka), Water Science and Technology Library, vol. 2, pp. 67–82. Springer.

HUNT, J. C. R. & GRAHAM, J. M. R. 1978 Free-stream turbulence near plane boundaries. *J. Fluid Mech.* **84** (2), 209–235.

ITSWEIRE, E. C., KOSEFF, J. R., BRIGGS, D. A. & FERZIGER, J. H. 1993 Turbulence in stratified shear flows: implications for interpreting shear-induced mixing in the ocean. *J. Phys. Oceanogr.* **23** (7), 1508–1522.

IVEY, G. N. & IMBERGER, J. 1991 On the nature of turbulence in a stratified fluid. Part I: the energetics of mixing. *J. Phys. Oceanogr.* **21**, 650–658.

IVEY, G. N., WINTERS, K. B. & KOSEFF, J. R. 2008 Density stratification, turbulence, but how much mixing? *Annu. Rev. Fluid Mech.* **40** (1), 169–184.

KOMORI, S., NAGAOSA, R., MURAKAMI, Y., CHIBA, S., ISHII, K. & KUWAHARA, K. 1993 Direct numerical simulation of three-dimensional open-channel flow with zero-shear gas–liquid interface. *Phys. Fluids* A **5**, 115–125.

KOMORI, S., UEDA, H., OGINO, F. & MIZUSHINA, T. 1983 Turbulence structure in stably stratified open-channel flow. *J. Fluid Mech.* **130**, 13–26.

KULLENBERG, G. E. B. 1976 On vertical mixing and the energy transfer from the wind to the water. *Tellus* **28** (2), 159–165.

LINDBORG, E. 2006 The energy cascade in a strongly stratified fluid. *J. Fluid Mech.* **550**, 207–242.

MONIN, A. S. 1970 The atmospheric boundary layer. *Annu. Rev. Fluid Mech.* **2**, 225–250.

MOSER, R. D., KIM, J. & MANSOUR, N. N. 1999 Direct numerical simulation of turbulent channel flow up to $Re = 590$. *Phys. Fluids* **11**, 943–945.

NAGAOSA, R. & HANDLER, R. A. 2003 Statistical analysis of coherent vortices near a free surface in a fully developed turbulence. *Phys. Fluids* **15** (2), 375–394.

NEZU, I. & RODI, W. 1986 Open-channel flow measurements with a laser Doppler anemometer. *J. Hydraul. Engng* **112** (5), 335–355.

NIEUWSTADT, F. T. M. 1984 The turbulent structure of the stable, nocturnal boundary layer. *J. Atmos. Sci.* **41** (14), 2202–2216.

NIEUWSTADT, F. T. M. 2005 Direct numerical simulation of stable channel flow at large stability. *Boundary-Layer Meteorol.* **116** (2), 277–299.

OSBORN, T. R. 1980 Estimates of the local rate of vertical diffusion from dissipation measurements. *J. Phys. Oceanogr.* **10**, 83–89.

POPE, S. B. 2000 *Turbulent Flows*. Cambridge University Press.

SHIH, L. H., KOSEFF, J. R., IVEY, G. N. & FERZIGER, J. H. 2005 Parameterization of turbulent fluxes and scales using homogeneous sheared stably stratified turbulence simulations. *J. Fluid Mech.* **525**, 193–214.

SIMPSON, J. H., ALLEN, C. M. & MORRIS, N. C. G. 1978 Fronts on the continental shelf. *J. Geophys. Res.* **83** (C9), 4607–4614.

SIMPSON, J. H. & HUNTER, J. R. 1974 Fronts in the Irish sea. *Nature* **250**, 404–406.

SMYTH, W. D. & MOUM, J. N. 2000 Length scales of turbulence in stably stratified mixing layers. *Phys. Fluids* **12**, 1327–1342.

SORBJAN, Z. 1986 On similarity in the atmospheric boundary layer. *Boundary-Layer Meteorol.* **34** (4), 377–397.

SORBJAN, Z. & GRACHEV, A. A. 2010 An evaluation of the flux-gradient relationship in the stable boundary layer. *Boundary-Layer Meteorol.* **135** (3), 385–405.

TAYLOR, J. R., SARKAR, S. & ARMENIO, V. 2005 Large eddy simulation of stably stratified open channel flow. *Phys. Fluids* **17** (11), 116602.

WANG, L. & LU, X.-Y. 2005 Large eddy simulation of stably stratified turbulent open channel flows with low-to high-Prandtl number. *Intl J. Heat Mass Transfer* **48** (10), 1883–1897.

WIEL, B. J. H., MOENE, A. F., RONDE, W. H. & JONKER, H. J. J. 2008 Local similarity in the stable boundary layer and mixing-length approaches: consistency of concepts. *Boundary-Layer Meteorol.* **128** (1), 103–116.

ZONTA, F., ONORATO, M. & SOLDATI, A. 2012 Turbulence and internal waves in stably-stratified channel flow with temperature-dependent fluid properties. *J. Fluid Mech.* **697**, 175–203.